DETERMINATION OF 3-D BORON DISTRIBUTION

by

ABOLGHAASEM FADAAI

B.S. (Met.E.), Arya Mehr University
(1976)

SUBMITTED IN PARTIAL FULFILLMENT
OF THE REQUIREMENTS FOR THE
DEGREES OF

MASTER OF SCIENCE IN NUCLEAR ENGINEERING

and

MASTER OF SCIENCE IN MATERIALS SCIENCE AND ENGINEERING

at the

MASSACHUSETTS INSTITUTE OF TECHNOLOGY

JUNE 1978

Signature redacted

Signature of Author .....
Department of Nuclear Engineering,
June 28, 1978

Signature redacted

Certified by .. 6/28/78 .....
Thesis Supervisor

Signature redacted

Certified by .....
Thesis Supervisor

Signature redacted

Accepted by .....
Chairman, Department Committee on
Graduate Students

DETERMINATION OF 3-D BORON DISTRIBUTION

by

ABOLGHAASEM FADAAI

Submitted to the Department of Nuclear Engineering on June 28, 1978 in partial fulfillment of the requirements for the Degrees of Master of Science in Nuclear Engineering and Materials Science and Engineering.

ABSTRACT

The technique of boron autoradiography has been used to study the spatial distribution of boron in splat cooled 316 stainless steels. The products from the $^{10}B(n,\alpha)^{7}Li$ reaction produce tracks in a cellulose acetobutyrate replica exposed to a thermal-neutron flux while in contact with the specimen. The tracks are revealed by etching in aqueous KOH at 50°C. Track density is proportional to boron content. A track size of $\sim$ 0.2 μm is obtained when the replica is etched in 50% KOH at 50°C for 10 minutes. A resolution of $\sim$ 0.3 μm is obtained if the replica is studied in a TEM, making the technique capable of studying boron distribution in small-grained materials.

For splat cooled specimens of stainless steel containing as high as 500 appm boron no detectable segregation was observed. This was also true for specimens which were heated for 90 minutes at 575°C. Presence of precipitates in the specimens is believed to be due to different impurities, such as S and O, and not because of boron. Electron energy loss spectrometry attached to a STEM didn't detect any boron in the precipitates.

The final conclusion supported by both boron autoradiography and electron microscopy, is that a uniform distribution of

boron is obtained if the ss alloy, containing as high as 500 appm B, is splat cooled from the melt.

Thesis Supervisor: O. K. Harling
Title: Director of MIT Research Reactor

Thesis Supervisor: N. J. Grant
Title: Professor of Metallurgy

TABLE OF CONTENTS

LIST OF FIGURES

LIST OF TABLES

ACKNOWLEDGEMENTS

I would like to express my sincere appreciation to Professor O. K. Harling and Professor N. J. Grant for their valuable guidance and patience throughout the course of this research.

A special note of appreciation is given to Miss. S. West, who prepared the splat cooled alloys.

I would also like to thank the staff of the M.I.T. Reactor for their cooperation in carrying out the research.

CHAPTER 1

INTRODUCTION

Controlled thermonuclear reactor (CTR) is considered to be a major source of energy for the future. Research is going on in different fields of CTR development. An important part of this work is the development of proper materials which will be used in fusion power reactors.

The structural components of a CTR, especially its first wall, will be subjected to a very severe high temperature and irradiation environment for long periods of time. The safe and economic operation of a CTR will, to a large extent, depend on how successfully materials are chosen that can retain adequate mechanical and physical properties under such severe conditions.

Many materials problems associated with fusion reactors have become apparent through reactor design studies and experiments in conventional fission reactors. Such studies have shown that simultaneous generation of radiation damage and helium is one of the most important problems which must be resolved before construction of commercial fusion reactors.

It is obvious that we must know the quantitative values of the displacement and transmutation rates in

potential CTR materials. Since high power fusion reactors will not be available until at least the late 1980s,[1] therefore we must try to simulate reactor conditions the best we can in current irradiation facilities and test the potential materials under these simulated conditions to see if they will meet the design requirements.

Doran, Kulcinski, and Abdu[2] have calculated gas and damage production rates for several CTR designs. Their calculated results for five suggested materials in different nuclear facilities are given in Tables 1.1 and 1.2 and Figures 1.1 and 1.2. The displacement rates in the first wall of a fusion system vary from a low of 2.3×10^{-7} dpa/s

Table 1.1.--Calculated helium production rates for typical nuclear facilities (after Kulcinski et al.).

	appm/s × 10^7					
	316 SS[a]	316 SS[b]	Cb	MO	V	SAP
CTR (1 MW/m^2)	64	N	7.6	15	18	130
FFTF	2.5	N	0.53	0.95	0.15	5.5
EBR-II	1.5	N	0.31	0.57	0.097	2.5
HFIR	2.6	1330	0.57	1.0	0.15	5.8
ETR	0.61	48	0.15	0.27	0.030	1.3
RTNS	2.9	N	0.34	0.68	0.81	5.9
LAMPF	5.1	N	0.62	1.2	1.3	9.1

[a]Primary reactions only.

[b]Helium (appm/s × 10^7) contribution from $^{58}Ni(n,\alpha)^{59}Ni(n,\alpha)$ after one year of irradiation.

N = negligible.

Table 1.2.--Calculated maximum displacement rates for typical nuclear facilities (after Kulcinski et al.).

	dpa/s × 10^7				
	316 SS	Cb	Mo	V	Al
CTR (1 MW/m^2)	3.1	2.3	2.6	3.7	5.4
FFTF (400 MW)	26	16	19	34	49
EBR-II (62.5 MW)	14	9.0	9.6	17	24
HFIR (100 MW)	14	7.8	8.4	16	19
ETR (175 MW)	5.1	3.2	3.5	6.6	8.4
RTNS (2 × 10^{12} n/cm^2 /s, 14 Mev)	0.14	0.1	0.12	0.12	0.24
LAMPF (2 × 10^{14}n/cm^2 /sec, total)	0.84	0.6	0.6	1.1	1.4

to 5.4 × 10^{-7} dpa/s in aluminum. In all cases considered in these calculations, fission reactors yielded higher displacements rates than that expected for a CTR first wall and blanket at 1 MW/m^2 wall loading. For the gas production rates (especially He) the situation is much different and there are dramatic differences between the gas production rates of various materials in the same reactors. The more important point is that the helium production rate is much greater in a CTR first wall than in the current fission radiation facilities. In fact, nonfusion sources cannot generate enough helium to duplicate the production rates in the first 40 to 50 cm of such a blanket. On the other hand, fission reactors may be able to duplicate the helium production rates up to $\sim$ 7 MW/m^2 by the use of various tracks.

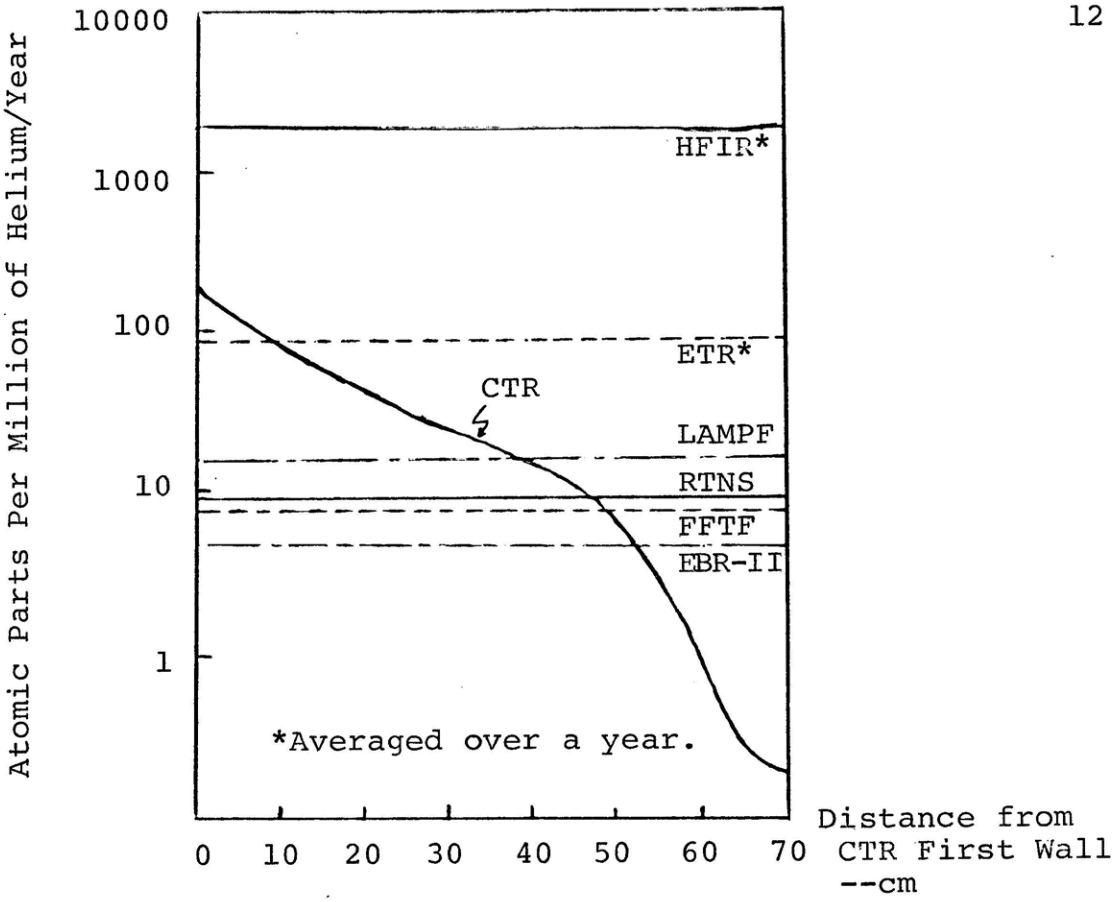

Figure 1.1.--Calculated helium production rate in Type 316 stainless steel for various nuclear facilities (after Kulcinski et al.).

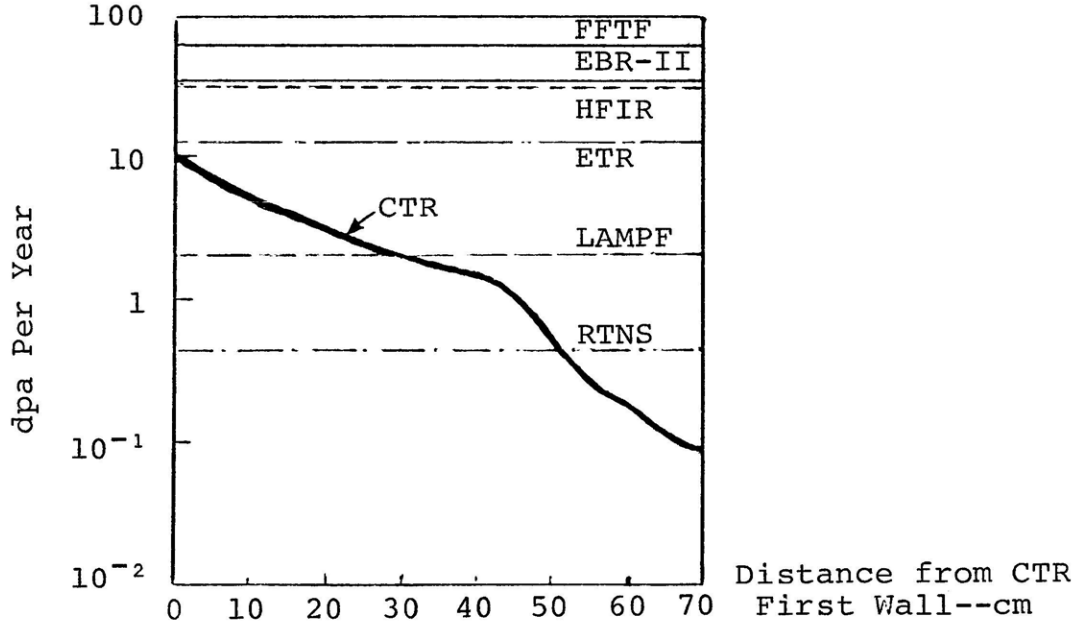

Figure 1.2.--Displacement rate in 316 SS for various nuclear facilities assuming a 100% plant factor. Fusion reactor has a first wall loading of 1 MW/m^2 (after Kulcinski et al.).

The problem of duplicating CTR helium generation rates in a fission reactor is the major difficulty in simulation of CTR conditions. The important parameter is the helium to displacement ratio which has to be simulated in the conventional facilities. Figure 1.3 shows the calculated ratio for different materials in different facilities. It shows that for most CTR designs the ratio is between 7:1 appm He/dpa and 15:1 appm He/dpa.

Existing irradiation facilities are not capable of simulating the proper ratio of helium to dpa. Table 1.3[3] summarizes the features of some existing facilities. In order to overcome the main difficulty, which is helium generation, different "tricks" have been used and some of them are shown in Table 1.4.[3] Doping with boron or lithium is one of the techniques used. The biggest problem with boron doping of conventional ingot alloy products is the segregation and precipitation of boron at grain boundaries which subsequently affects the mechanical properties of the materials.[4] Furthermore, we must get a uniform distribution of generated helium in the material. Since the purpose of boron doping is to provide a mechanism for synergistic helium and damage production, it is important that the boron be homogeneously distributed throughout the alloy at least on the scale of the alpha particle range, i.e., 1-2 μm. The use of rapid quenching from the melt offers the possibility of a uniform distribution of boron at a useful concentration.

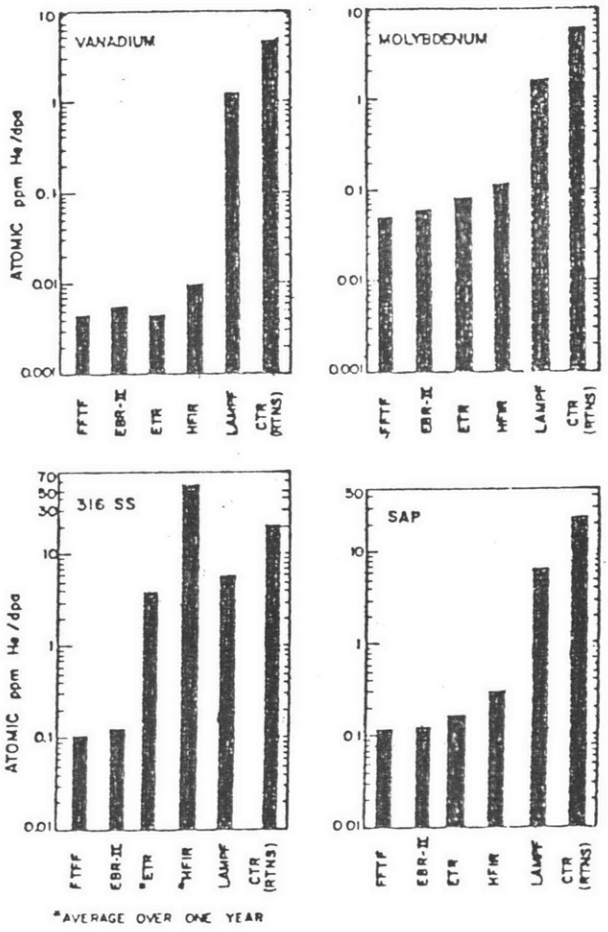

Figure 1.3.--Calculated helium to displacement ratio in various nuclear facilities (after Kulcinski et al.).

Table 1.3.--Existing irradiation facilities for potential use in CTR first wall studies

Facility	Positive Features	Negative Features
A. Fission reactors		
1. High flux mixed spectrum reactors ($\phi \geq 1 \times 10^{14}$ n/cm^2 sec of fast neutrons and thermal neutrons).	1. Can produce dpa and helium at real time up to $\sim$ 2 MW/m^2 and at accelerated rates below this in for alloys containing nickel. 2. Instrumentation available to actively control during irradiation the temperatures, stresses, and chemical environments relevant to CTRs. 3. Can conduct in situ measurements. 4. Have the large experimental volume necessary for the required test matrix. 5. High duty factor.	1. Does not match CTR neutron energy spectrum. 2. Can't product relevant helium concentrations in materials that do not contain nickel.
2. Fast neutron reactors	1. Can produce dpa greatly accelerated over that in a CTR at 1 MW/m^2. 2. Large experimental volume. 3. Passive temperature and stress control; active control may be possible later. 4. Good simulation of the CTR neutron energy spectrum for regions beyond the first wall.	1. Can't produce relevant helium concentrations in any structural material. 2. No capability for in situ measurements. 3. Currently no active control of temperature and stress of chemical environment.
B. Ion accelerators	1. Highly accelerated dpa rates, good for swelling studies. 2. Can actively control temperature, stress, and chemical environment. 3. Can conduct in situ measurements.	1. Extremely difficult to conduct mechanical properties studies. 2. Time dependence of kinetic processes must be established.

CTR Annual Report, July 1976 (J. A. Horak).

This can be done by splat cooling with cooling rates up to 10^6 °C/s.

This new boron doping technique has been suggested by Professor O. K. Harling, Director of M.I.T. **Reactor Laboratory**, and its study has been approved by the U.S. Department of Energy. In order to carry out the project, techniques for the determination of the boron distribution must be established. Establishing the techniques for 316 stainless steels (316 SS) and similar materials is the objective of this thesis. This is one of the first tasks of the approved project.

Boron autoradiography has been found to be a useful tool to study boron distribution. It has proved successful for slow cooled alloys with a grain size of the order of 50 μm. In this work we have tried to apply this technique to splat cooled 316 SS, and to optimize the resolution to make the technique useful for fine grain sizes. In Chapter 2 we will discuss different aspects of boron autoradiography technique.

Chapter 3 covers different electron microscopy techniques used for direct examination of specimens. Particle extraction techniques will also be covered in this chapter. In Chapter 4 results will be discussed and compared. Chapter 5 covers the summary of the whole work.

Table 1.4.--Different tricks used to simulate CTR environment.

Method	Description of Approach	Advantages	Disadvantages
Nickel Trick	Miscellaneous spectrum reactors provide: • Helium from the 2 stage $^{58}Ni^{2n} \rightarrow He + {}^{56}Fe$ reactions. • Moderate displacement rates from the high energy portion of the neutron spectrum.	• With some flux tailoring (such as that proposed at ORR) a good He/dpa ratio can be achieved and maintained.	• Only for use with Ni bearing alloys.
Fast Reactor Irradiations	• EBR-II FTR • Some helium generated from threshold (n,α) reaction. High displacement rates from hard neutron spectrum.	• High displacement rates allow accelerated testing. • Large irradiation volumes available.	• Inadequate quantity of helium generated.
Single Beam Accelerators	• Damage produced by high energy heavy or light ions. • Helium preinjected by α-particles bombardment or tritium decay.	• Low activation of specimens. • Good instrumentation possible. • High damage rates available. • Good for study of fundamental mechanisms.	• Small damage volume with uniform damage rate. • He and damage generated separately. • Difficulty correlating neutron and ion damage (different PKA spectrum).
Dual Beam Accelerator	• Helium produced by alpha particle beam. • Damage produced by high energy heavy or light ions.	• Same as for single beam experiments. • Produce helium and damage simultaneously. Can easily vary He/dpa ratio.	• Small damage volume. • Difficult to correlate neutron and ion damage results.
"Tritium Trick"	• Helium produced by diffusing tritium into the material at higher temperatures. Tritium decays with $t_{1/2}$ = 12.3 years. • Damage produced by ion beam bombardment or fast reactor irradiation.	• Provides a source of helium for irradiation or bombardment experiments which do not generate adequate amounts.	• Difficult to control the distribution of the tritium (and thus the helium). • Introduction of tritium may cause hybriding in some materials. • Helium and damage are not produced simultaneously.
Preinjection of Helium	• Helium is injected into the material prior to irradiation by alpha particle bombardment. • Damage produced by ion beam bombardment or fast neutron irradiation.	• Same as for "Tritium Trick."	• Sample volumes prepared in this manner are small. • Helium and damage are not produced simultaneously.
Doping with Fissionable Material	• Damage rate enhanced by doping material with fissionable material and then irradiating in a thermal or mixed-spectrum reactor. Fission fragments generate a great amount of damage. • Helium is generated from (n,α) reactions in the sample and, in small quantities, from nuclear fission.	• Permits establishment of high damage rates in reactors having soft neutron spectra. • Helium and damage may be created simultaneously and in the correct ratio.	• Difficult to account for the physical and chemical effects of the fission products. • Difficult to uniformly distribute the fissionable material.
Conventional Doping with Boron or Lithium	• Utilizes mixed spectrum reactors. • Helium is produced by the thermal neutron reactions $^{10}B(n,\alpha)^{7}Li$ or $^{6}Li(n,\alpha)^{3}H$. • Damage is produced in moderate amounts by the fast component of the neutron spectrum.	• Permits simultaneous generation of helium and displacements.	• Difficult to uniformly distribute the boron or lithium. • Difficult to account for the effects of boron or lithium on preirradiation materials. • Difficult to prevent segregation of boron to grain boundaries.

CHAPTER 2

BORON AUTORADIOGRAPHY

2.1 Particle Track Etching

The passage of heavily ionizing, nuclear particles through the most insulating solids creates narrow paths of intense damage on an atomic scale. These damage tracks can be revealed and seen in an optical microscope if they are treated with a properly chosen chemical reagent that preferentially attacks the damaged zones. This simple technique has been used in a wide variety of technical fields. Figure 2.1 shows the envisioned character of tracks in crystalline and polymeric solids.

The first direct photographs of damage trails created by ^{235}U fission fragments were TEM micrographs of mica[5] published in 1959. Since then, this technique has found diverse applications in science and technology. The applications range from semiconductor electronics to aerosol sampling, identification of microbiological particles, nuclear engineering, mine safety, neutron radiography, uranium exploration, sewage disposal, and securing nuclear reactors for safety use. Fission track dating is a powerful tool for age measurements of natural minerals.[6] Determination of the distribution of plutonium and other transuranium

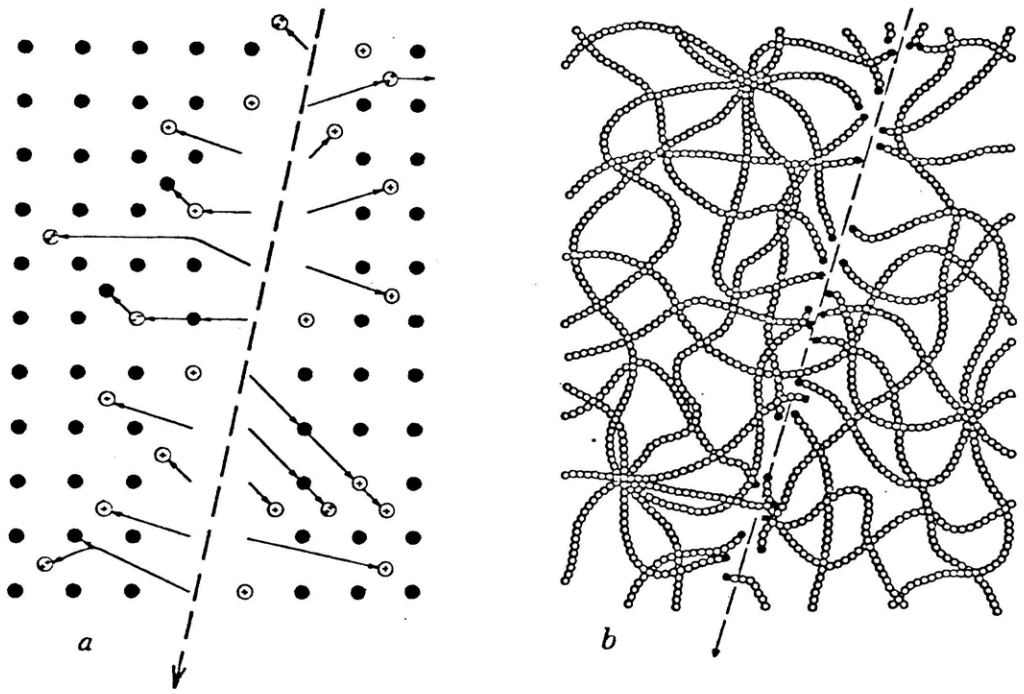

Figure 2.1.--The atomic character of a particle track in (a) a crystal and (b) a polymer. In the crystal the damage consists of continuous disorder composed of vacant lattice sites and of interstitial ions or atoms. In the polymer new chain ends and other chemically reactive sites are formed (after Fleischer et al., 1969).

elements in bone tissue[7] in another application of particle track etching technique. A most recent application is the study and measurement of sputtering of uranium[8,9] and some other elements[10] by different ions. Study of the boron distribution in different alloys has its own importance both in nuclear technology and in metallurgy. Table 2.1 summarizes[11] the different applications of this technique.

In recent years it has become recognized that the presence of boron up to ppm level in steels and other alloys can greatly influence physical and mechanical properties of these materials.[12] As examples, boron has important effects on steels used for nuclear-reactor construction,[13] and on creep,[14,15] fracture,[16] and other properties of steels. The low atomic number of this element has made it very difficult to determine its content with an electronprobe microanalyzer. There was, therefore, a need for new methods of determining boron distribution on a microscopic scale in order to understand its behavior.

Hughes and Rogers[17] were the first people who developed the boron autoradiography technique to overcome the difficulty in determining boron distribution. The technique is based on the ability of some plastics to record the passage of charged particles of certain energies and in this case use is made of the reaction of the ^{10}B isotope with thermal neutrons which results in the production of one helium and one lithium ion for each boron that undergoes

Table 2.1.--Diverse applications of etched particle tracks

Science	Application
Anthropology	Age of Bed , Olduvai Gorge. Age of man-made glasses. Uranium in fossil bone.
Archaeology	Uranium content of ancient glasses.
Astrophysics	Ultraheavy cosmic rays: abundance measurements. Detection of ^{244}Pu in early solar system.
Avionics	Flight times and altitudes of birds.
Biophysics	Size, count, and identify bacteria, viruses, and other small particles.
Botany	Distribution of boron in leaves.
Cosmic Ray Physics	Identification of heavy cosmic rays. Energy spectrum of heavy solar flare particles.
Chemistry	Distribution and quantity of fissionable elements [or those with (n,α) reactions] (U, Th, Pu, Li, B, N, O).
Cytology	Isolation of malignant cells.
Elementary Particle Physics	Magnetic monopole searches.
Geochemistry	Distribution in nature of U, B, Li.
Geochronology	Fission track dating.
Geophysics	Measure rate of ocean bottom spreading in N. Atlantic.
Membrane Physics	Flow behavior in fine holes.
Metallurgy	Locate impurities and boron-rich precipitates in metallurgical structures.
Meteoritics and Selenology	Erosion and ablation of meteorites. Early chronology and thermal history. Surface exposure times on moon. Accretion, erosion, and stirring on the moon.
Nuclear Physics	High resolution particle identification. Study heavy particle reactions. Measure cross-sections, lifetimes. Spallation studies.
Radiation Biology	Heavy particle exposure of astronauts.
Solid State Physics	Neutron-sensitive plate for neutron diffraction studies. Defect identification, channeling, and blocking studies. Nature of particle tracks in solids.
Superfluidity	Test understanding of superfluid rock through small, uniform holes.
Superconductivity	Behavior of fine wires of known geometry.
Solar Physics	Energy and composition of solar nuclei.
Accelerator Engineering	Beam attenuator for Superhilac.
Alloy development	Structure of new superconducting alloys.
Altimetry	Integrating barometer.
Dosimetry	Count neutrons, protons, heavy particles.
Environmental studies and Radiation Protection	Aerosol filtration. Personnel radiation dosimetry. Personnel dosimetry in space. Nuclear detonation detection. ^{239}Pu detection in bone, urine, etc. Uranium measurements in water supplies. Tracer studies on sewage distribution in ocean waters.
Filtration	Nuclepore filters for cytology, bacteria removal, etc.
Gem diamond manufacture	Boron and nitrogen distributions mapped in relation to color.
Imaging	Neutron, proton, and heavy ion radiography.
Medical technology	DeBlois-Bean virus counter; diagnostic radiography.
Nuclear engineering	Leak detection in fuel rods. Neutron dosimetry. α-Radiography to give Pu-U distribution in fuel rods. ^{239}Pu particle size analysis.
Uranium exploration	^{222}Rn emanation mapping.

fission. If the ions are allowed to impinge upon an appropriate plastic detector before they have lost too much energy, then they leave a damage trail in the plastic identifiable by subsequence chemical treatment.

The plastic detectors have to be insensitive to other radiations such as gamma and beta rays and neutron radiations. A number of plastics have found suitable as detectors for low energy α-particles and the best include cellulose nitrate and cellulose acetobutyrate (CAB). In general, the sample is mounted and polished and then placed in close contact with a film of plastic detector. The assembly is heated and then exposed to a suitable source of thermal neutrons. Then the film is removed and etched to reveal the tracks. Figure 2.2 shows the paths of the α-particles.

This technique has found many applications in physical and mechanical metallurgy and also in nuclear materials research. Boron segregation to grain boundaries and its precipitation have been successfully studied by using this technique.[18-21] Another application is quantitative analysis of boron in solids,[22] which is based on track density measurement in the plastic film. Track density is directly proportional to the boron content of the material. The best accuracy is $\pm$ 10% for concentrations of boron greater than 30 ppm. The errors are larger at lower levels of boron (due to the increasing background).

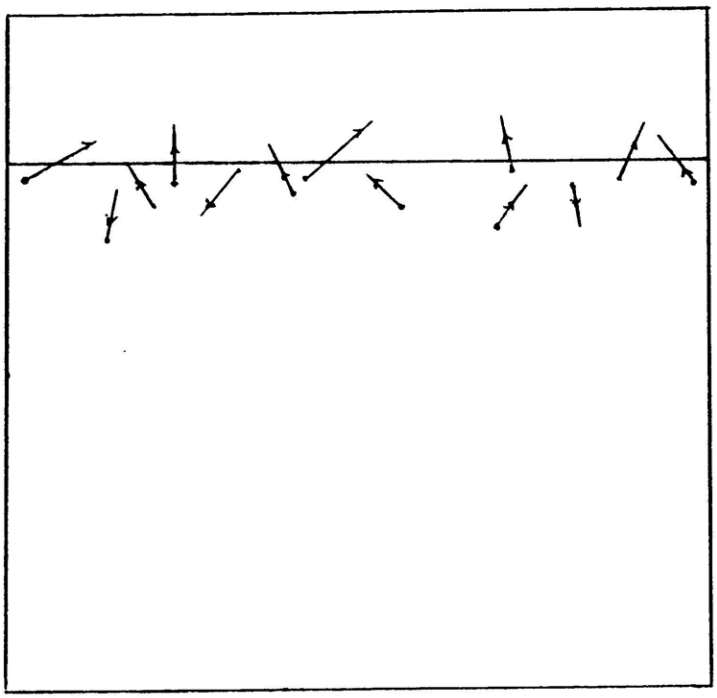

Figure 2.2.--α-particles with their paths at specimen-plastic film interface.

Recently, boron autoradiography has been adopted as the major analytical tool in a collaborated projected with the University of Cambridge to determine the solubility of boron in high-purity iron.[23] The results are shown in Figure 2.3. The work has been extended to determine the effect of other interstitial elements on boron solubility.

2.2 Helium Ion Formation

Natural boron contains 18.8 % ^{10}B and 81.2% ^{10}B. The lighter isotope reacts with thermal neutrons with a high cross-section of 3840 barns. The boron fission reactions are[24]:

$$^{10}B_5 + {}^{1}n_0 \begin{cases} 93.7\% \longrightarrow {}^{7}Li_3\ (0.83\ \text{Mev}) + {}^{4}He_2\ (1.48\ \text{Mev}) \\ 6.3\% \longrightarrow {}^{7}Li_3\ (1.01\ \text{Mev}) + {}^{4}He_2\ (1.79\ \text{Mev}). \end{cases}$$

So, in a constant thermal flux, the change of boron-10 concentration with time is

$$\frac{dC_B}{dt} = - C_B \cdot d \cdot \phi_{th} \qquad (1)$$

where ϕ_{th} is the thermal neutron flux, d is the reaction cross-section, and C_B is the concentration of boron-10 in the sample. If $\dot{C_B}$ is the initial concentration of boron-10, the concentration of boron-10 at time t is

$$C_B = \dot{C_B} \exp(- d \cdot \phi_{th} \cdot t). \qquad (2)$$

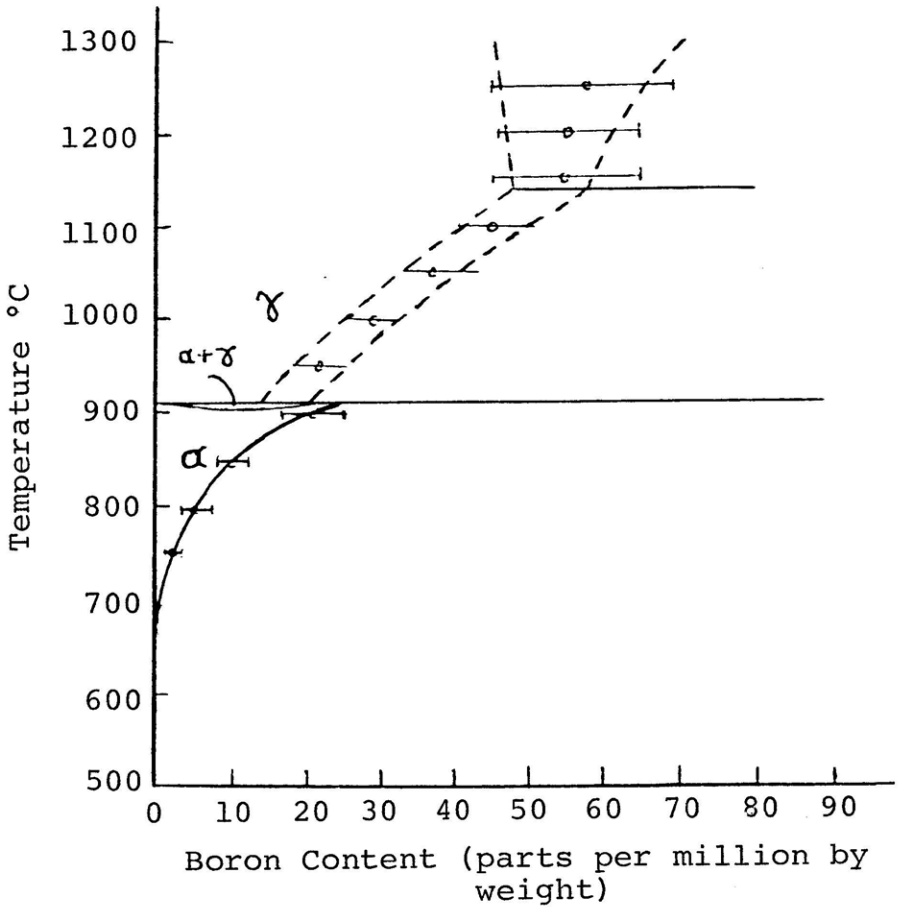

Figure 2.3.--The solid solubility of boron in high-purity iron as determined by boron autoradiography.

And, if $\dot{N}_B$ is the initial number of boron-10 atoms, the number of boron-10 atoms at time t is

$$N_B = \dot{N}_B \exp(- d \cdot \phi_{th} \cdot t) \tag{3}$$

and the number of α-particles produced is

$$N_\alpha = \dot{N}_B \left[1 - \exp(- d \cdot \phi_{th} \cdot t)\right]. \tag{4}$$

For all of the boron autoradiography experiments, the product of $d \cdot \phi_{th} \cdot t$ is much less than unity, so the number of α-particles can be approximated by

$$N_\alpha = \dot{N}_B \cdot d \cdot \phi_{th} \cdot t. \tag{5}$$

The track density, ρ_t, in the plastic detector is proportional to the total number of ^{10}B fissions which have taken place; thus the track density can be presented as

$$\rho_t = K \cdot \dot{N}_B \cdot \phi_{th} \cdot t \tag{6}$$

where K is a constant which can be experimentally measured for different materials. In addition to α-particles, lithium ions make some contribution to the track density.

Fortunately, only three other naturally occurring isotopes have significant n,α cross-sections for thermal neutrons, namely ^{6}Li, ^{17}O, and ^{32}S, which generally give no significant contribution to ρ_t. On the other hand, major elements in steels have significant n,α cross-sections for

fast neutrons, thus for radiography experiments, the fast component of the neutron flux has to be kept as low as possible.

The range of the 1.48 and 1.79 Mev α-particles have been calculated in different materials, using those methods in conjunction with the known range of these particles in air[25] (0.73 and 0.88 cm, respectively). From the results, it appears that the average range of α-particles produced from boron-10 fissions is about 2.4 μm for steels. The range is about 1.2 μm for lithium particles.

2.3 Diameter of the Damaged Zone

Characterizing the extent of the most intensely damaged region of the core is an important step in the understanding of the nature of a particle track. Transmission electron microscopy gives upper limits on the diameter of the region of intense damage along fission particle tracks. TEM observations give a value of ∿ 50 Å for mica.[26] The most detailed and quantitative evaluation of diameters come from measurements by C. P. Bean and co-workers of electrical conductivity across thin detector membranes while transverse particle tracks are being etched through them. Typical results on mica give a radius of 33 Å. The same technique gives a radius of 100-200 Å for plastic detectors.[27]

2.4 Track Formation Mechanism

Particle tracks are narrow, stable, chemically reactive centers of strain that are composed mainly of displaced atoms rather than of electronic defects. They are not formed in good electronic conductors. Any detailed theory of how tracks form must fit this information.

2.4.1 General Description of Heavy Ion Energy Deposition in Solids

A fast atom of atomic number z moving through a solid would rapidly become an ion by being stripped of all or some portion of its orbital electrons. This stripping is a result of interaction of the electrons surrounding the moving atom and those around the atoms that make up the solid. From these interactions the ion gets a net positive charge z^*, an empirical form for which is given by[28]

$$z^* = z[1 - \exp(1 - 130\ \beta/z^{2/3})] \qquad (7)$$

where β is the speed v of the ion relative to that of light. In moving in the solid, the ion undergoes two types of collisions; at high speeds, where $z^* \approx z$, the dominant interaction is the electrical force between the ion and the electron. This force either 1) excites electrons to higher energy levels or 2) loosens them from their atoms and ejects them. In any solid process (2), ionization creates charge centers. The ejected electron, called a delta ray, can produce further excitation and ionization if it carries enough energy. The

original or primary ionization and excitation occur close to the path of the ions while the secondary ionization and excitation are spread over larger radial distances from the core of the track.

When an ion slows down in passing through the solid, atomic collision becomes important. Below $\sim$ 50 Kev/amu atomic collisions become the more dominant mode of energy loss. Many theories based on the partition of energy into atomic and electronic stopping have been developed.[29]

It is important to know the relative importance a) of the primary damage that results from the excitation and ionization caused by heavy ions and b) of that part of the secondary damage that is caused by delta rays during their passage close to the path of the ion. For inorganic solids, such as detectors, the secondary effects of delta rays are unimportant, and primary ionization appears to be the major source of track damage.

For plastics, such as cellulose acetate butyrate, the effect of delta rays cannot be neglected. It has been shown by different measurements and calculations that the damage-track-radius is $\sim$ 100 to 200 Å, well outside the region of primary excitation and ionization. It is not known definately what the relative importance of primary ionization is for polymers, but it is probable that both primary and secondary ionization contribute in the polymers and consequently will need to be considered in a complete theory, which is not

developed yet. Primary plus secondary damage theory[30] has given a promising set of calculations which has started to provide a complete theory about the energy distribution around a particle track. This theory has found that the proportion of energy loss in primary processes is about 40% of the total at 1 Mev/amu and diminishes monotonically with increasing energy to 30%, 25%, and 20% at 10 Mev/amu, 100 Mev/amu, and 1000 Mev/amu, respectively. A book by Fleischer et al.[11] gives more details about track formation mechanisms and the different theories suggested.

2.5 Experimental Procedure

Specimens for examination were as small as possible, generally 3 x 3 x 0.2 mm, to minimize the total radioactivity induced in them. They were mounted in fully cured bakelite, which has a very low neutron-absorption cross-section, is insoluble in methyl isobutyl ketone, and can withstand a temperature as high as 150°C. If the bakelite was not fully cured, the films adhered tenaciously to it. The specimens were then polished by standard metallographic polishing procedures.

The plastic detector was cellulose acetate butyrate (CAB) with 17% butyryl content, bought from the Aldrich Chemical Company. The film was prepared from a 20 wt./wt. % solution of CAB in methyl ethyl ketone. A pool of solution was spread across a carefully cleaned microscopic slide by means of a clean, dry rod, as shown in Figure 2.4. The rod

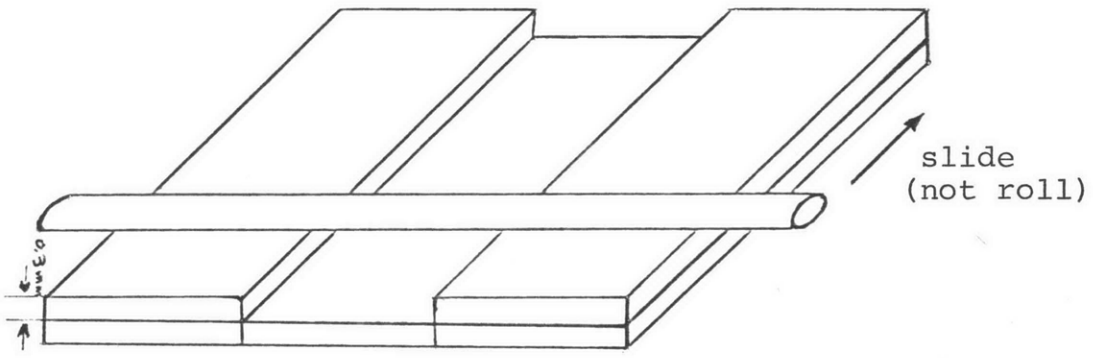

Figure 2.4.--Method of preparing the cellulose acetate butyrate film.

was pushed, not rolled, across the slide, producing flawless film less than 50 μ thick when dry. The film was dried in a horizontal position in a dust-free desiccator.

When dry, a small area of film was cut and detached from the slide. Then it was applied to the specimen surface using a minimum amount of methyl isobutyl ketone to give a good contact. The upper surface of the film was not wet with methyl isobutyl ketone as a perfect surface facilitated interpretation. A preliminary replication was performed to remove dust particles and clean the surface. The film on the specimen was dried in a desiccator. The assembly was then heated at 145° ± 2°C for at least one hour. Specimens (in polythene capsules) were then irradiated in 2pH2 facility of MITR-II. This facility has a thermal-neutron flux of 8.11×10^{11} n/sec • cm^2 and a very high ratio of thermal-neutron to fast-neutron flux (thermal: fast $\sim 3 \times 10^3$). The temperature in the facility is $\sim$ 42°C.

After irradiation the specimens were soaked in distilled water for a few minutes in order to remove the CAB film from it easily and without damage. For development, the film was floated image-side down in 50% KOH at 50°C for 5-30 minutes.

The film was washed in distilled water and dried, then it was mounted under cover slips held in position with adhesive-paper tape. The film was then directly examined in an optical microscope. Tracks were visible with a resolution of $\sim$ 1.5 μm. But this resolution was not high enough

for splat cooled 316 stainless steels which had a grain size of $\sim$ 2 μ. Thus use of transmission electron microscopy and scanning electron microscopy was considered to be helpful for better resolution. For study in an SEM the film was shadowed with a layer of gold which had a thickness of $\sim$ 300 Å. The film was then studied in an SEM which gave a fission track resolution of $\sim$ 0.7 μ.

The film was too thick to be directly examined in a TEM, but when it was dissolved overnight in methyl ethyl ketone, a sufficiently thin replica (probably of cellulose) remained. Thus was formed by a complex reaction at the plastic surface in contact with alkali. After rinsing with fresh solvent the cellulose replica was picked up on a general EM grid and examined at 2-20 K magnification at 100 Kev. The replica was not stable enough in the electron microscope but we were able to get good images of the tracks. Stability and ease of handling were increased, however, when the etched surface of CAB film was coated with 300 Å of gold or carbon by normal evaporation techniques before dissolution of the CAB film. A fission track resolution of 0.3 μ was achieved by using TEM.

CHAPTER 3

ELECTRON MICROSCOPY OF THE SPECIMENS

3.1 Direct Examination of Specimens

The electron microscope is a well-established research tool which is used to study the microstructure of various alloys and materials. Studying of splat cooled 316 SS made it necessary to use different electron microscopy techniques. In the early stages of this work, TEM indicated the presence of precipitates not only on grain boundaries, but inside grains. It was not possible to get a clear diffraction pattern because of the small grain size of the samples which resulted in severe line broadening; the amount of precipitated phases was on the low side.

Scanning transmission electron microscopy (STEM) was tried next. A Vacuum Generator Model (VG HB5) was used. This microscope is a powerful instrument with different micro-analysis attachments. Energy dispersive X-ray analysis permits the semiquantitative analysis of small volumes of a specimen by analysis of X-rays emitted when the electron beam strikes the specimen. With the microscope operating at 100 Kv, the technique is capable of detecting elements with atomic numbers z, greater than 10. The technique failed to detect boron (z = 5) in the precipitates which we ultimately

wish to characterize. However, it was able to detect other elements such as S and Si in some of the precipitates.

3.1.1 Specimen Preparation

The requirements for a crystalline electron microscope specimen are simple; it should be approximately parallel sided, thin (usually 500-5000 Å), and have a clean surface. The last requirement is particularly important for, apart from the obvious disadvantage of having a thin layer of nonrepresentative material on the specimen surface, such surfaces show no contrast and can reduce the transparency of a specimen due to strong diffuse scattering of the electrons.[31] The most widely used method for specimen preparation is electropolishing, which has been used in this research. The electropolishing solution consists of an oxidizing agent and a solvent for products of oxidation. The basic curve describing the performance of an electropolishing solution is shown in Figure 3.1. The part of curve 1 from a to b is associated with attack at the most reactive points on the anode. The segment cd represents the polishing plateau, where the anode rapidly develops a high polish. On the length de the polishing action is still maintained but the smoothness of the specimen tends to be damaged by gas evolution at the anodes which causes pitting of the specimen. The electropolishing used in this research was carried out on the plateau of curve 1.

The electropolishing solution and operating conditions for 316 SS are given in Table 3.1. The low temperature of

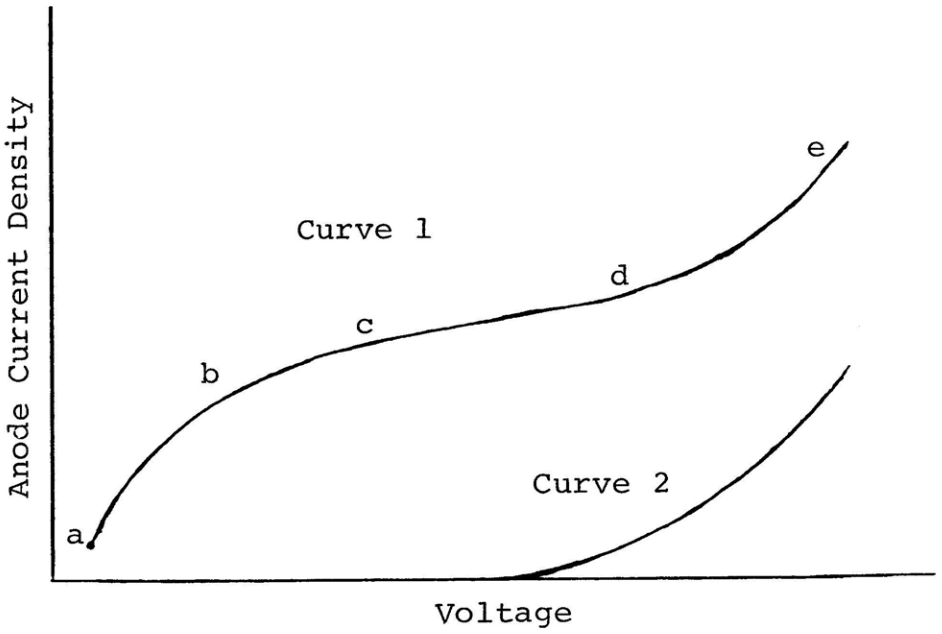

Figure 3.1.--A schematic illustration of voltage/current curve for a typical electropolishing solution with a metal anode (Curve 1) and an inert anode (Curve 2).

Table 3.1.--Electropolishing conditions for 316 SS

Electropolishing solution:	buthanol	150 cc
	methanol	250 cc
	perchloric acid	20 cc
Temperature:	T = -50°C to -40°C	
Voltage:	V = 22-24 v	
Time for polishing each specimen:	t = 5-10 minutes	

$\sim$ -50°C was attained by using a mixture of dry ice and acetone. After electropolishing, each specimen is washed in methanol and then dried on the filter and kept in a desiccator.

3.2 Particle Extraction Technique

Selective extraction of phases is a well established technique for the study of precipitates in materials. In this technique precipitates are extracted from the surface of a specimen and relocated on a carbon replica; then this replica is examined in an electron microscope. Because of various instrumental attachments on the STEM, this microscope was selected. Again the energy dispersive X-ray analysis was not able to detect boron in the particles. Therefore we tried electron energy loss spectrometry. The energy analysis of transmitted electrons gives an electron energy loss spectrum which may give useful information about the precipitates.

The technique has been able to detect boron in boron nitride[32] which contains about 40% boron. This technique is a new one at MIT and is still under development. No measureable boron signal was observable above the rather large background from the edge of the peak which contains electrons of the incident energy.

3.2.1 Extraction Replica Preparation Technique

The specimen (316 SS) was mounted in bakelite and then polished by standard metallographic polishing procedures. The specimen was then slightly etched in Kalling's Reagent (5 grams $CuCl_2$, 100 cc HCl, 100 cc Ethyl Alcohol, and 100 cc Distilled Water). The etching solution etches the matrix while precipitates may remain unetched. The specimen was then dried and shadowed with a $\sim$ 300 Å thick carbon film using a conventional vacuum evaporation technique. The carbon-shadowed specimen was then dropped in Kalling's Reagent, specimen side up. When the carbon film started to separate, the specimen was removed from the etching solution and dropped into distilled water. The carbon films which retain the particles and replicas of the surface of the sample were taken from the water, while being supported on general E.M. grids. The samples produced by this method were studied by STEM using electron energy loss spectrometry.

CHAPTER 4

RESULTS AND DISCUSSION

The work has been concentrated on reactor grade 316 austenitic stainless steel with various boron contents, mainly with 100 and 500 appm boron. This material was obtained from the Hanford Engineering Development Laboratory. The chemical composition of this alloy is given in Table 4.1.

Table 4.1.--Chemical composition of alloy used (316 SS).

Element	w/o	Element	w/o
C	0.005	Cu	< 0.01
Mn	1.52	Co	0.01
Si	0.54	V	< 0.005
P	0.001	Al	0.002
S	0.004	N	< 0.0005
Cr	17.29	Cb	< 0.01
Ni	13.69	Ta	< 0.015
Mo	2.26	As	< 0.005

The material was melted and the desired amount of boron was added to it. After being remelted several times to get a uniform distribution of boron, the alloy was quenched from the melt with a cooling rate of $\sim 10^6$ °C/sec, using the piston and anvil technique. The splat cooled samples had a thickness of $\sim$ 0.5 mm and a diameter of $\sim$ 5 cm. From splat cooled materials produced in this way, specimens for electron

microscopy, the extraction technique and boron autoradiography were made and studied.

4.1 Results of Electron Microscopy

All splat cooled specimens were found to have a grain size of about 2 μ. Samples with 100 and 500 appm boron were studied. Some work was also done on commercial 316 SS with 0.5% boron. The microstructure of splat cooled 316 SS with 100 appm boron content is shown in Figure 4.1, and the typical energy dispersive X-ray analysis of this alloy is shown in Figure 4.2. Different peaks correspond to different elements in the alloy, namely, Si, Mo, Cr, Mn, Fe, and Ni. As can be seen, boron and carbon because of their low atomic weight, and minor elements because of their low concentrations, are not detected. The presence of precipitates is easily seen in Figure 4.1. This is the case for all three different samples. In order to study and detect these precipitates STEM was used. The results can be summarized as follows:

1) Splat Cooled 316 SS + 100 appm B

At least two different precipitates were found. Bright field and dark field STEM images of the specimen are shown in Figures 4.3a and 4.3b, respectively. The size of the precipitates are as large as 1500 Å. All precipitates are rich in Si and Ti. Those which are bright in dark field images are also rich in Cr. In both precipitates Fe, Cr, and Ni are the major elements. The major difference between the

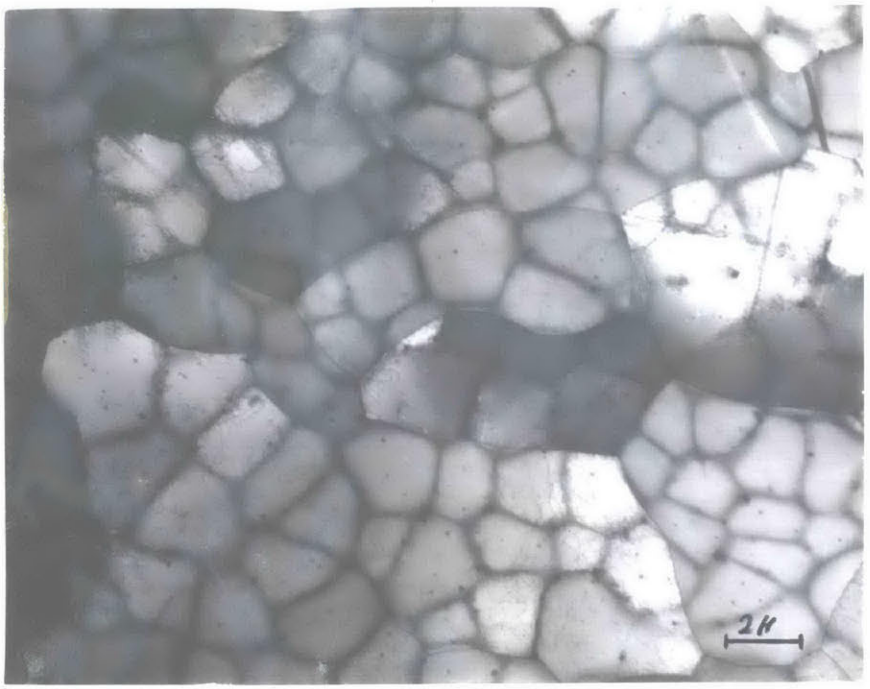

Figure 4.1.--Micrograph of a splat cooled 316 SS containing 100 appm boron taken by a TEM, 5000x.

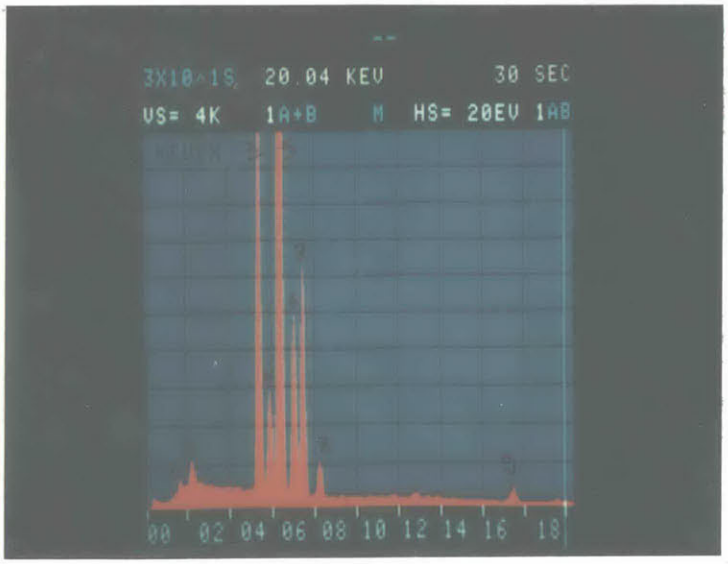

Figure 4.2.--Distribution of elements in 316 SS: 1) Si, 2) Mo (Lα), 3) Cr (Kα), 4) Mn (Kα), 5) Fe (Kα), 6) Fe (Kβ), 7) Ni (Kα), 8) Ni (Kβ), and 9) Mo (Kα).

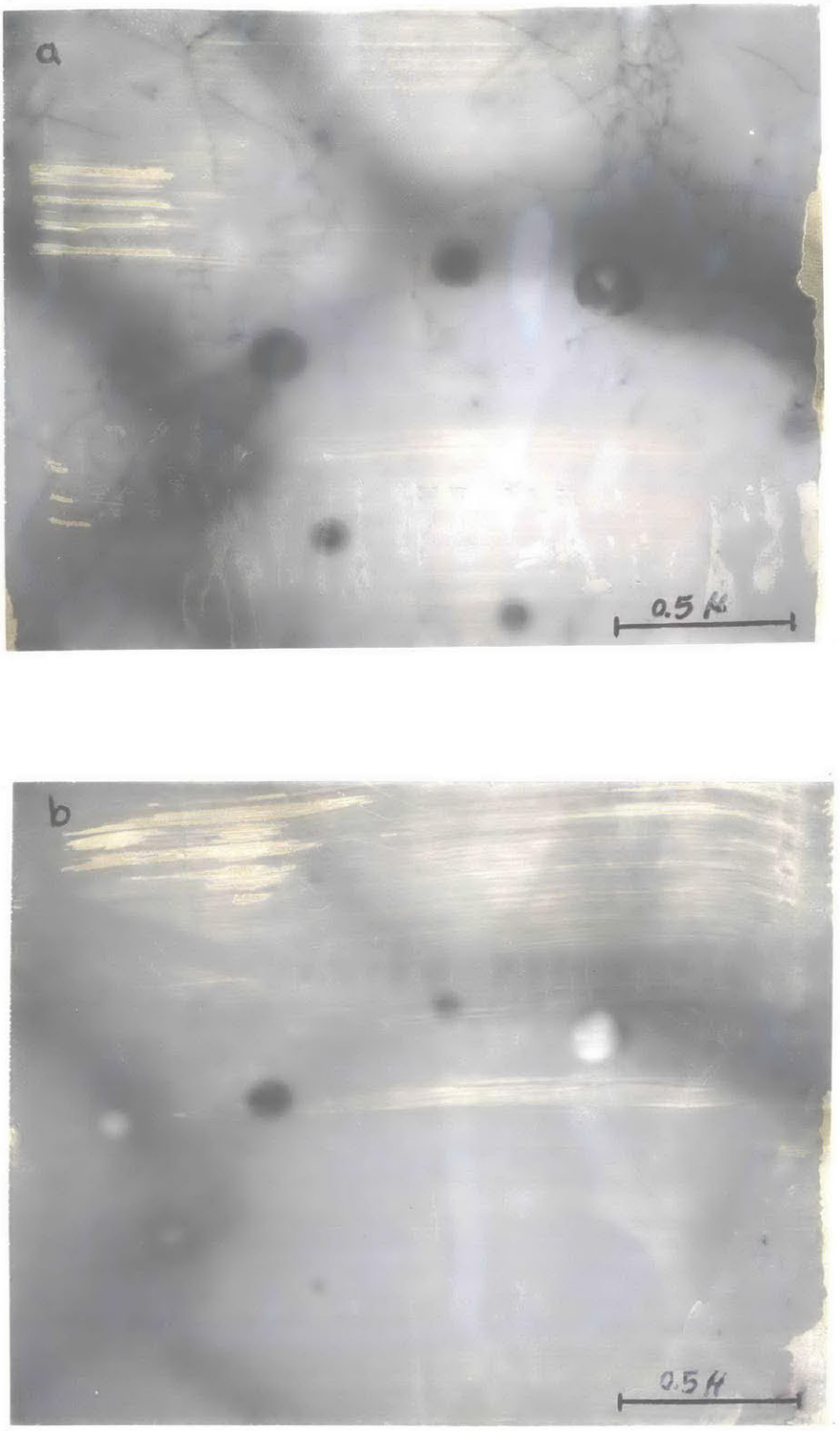

Figure 4.3.--STEM micrographs of splat cooled 316 SS with 100 appm B: a) bright field image, 5000x; b) dark field image, 5000x.

two kinds of precipitates comes from their chromium content. The first type of these precipitates has more chromium. Figure 4.4 shows energy dispersive X-ray analysis of the first kind of these precipitates. The six highest peaks represent Mo, Cr, Mn, Fe ($K_{\alpha 1}$), Fe ($K_{\beta 1}$), and Ni. These precipitates are found inside grains as well as on grain boundaries.

2) Splat Cooled 316 SS + 500 appm B

Samples with 500 appm B have fewer precipitates than samples with 100 appm B. The precipitates are smaller too, with a size not greater than $\sim$ 1000 Å. Bright field and dark field STEM images of a small part of the specimen are shown in Figure 4.5. Two different types of precipitates were found which are identical in Cr, Fe, and Ni content. Dark precipitates (in bright field) have more Mo than bright precipitates; both precipitates have significant amounts of Si and probably S in them. Also, an individual large precipitate ($\sim$ 0.3 μ) was found which was very rich in Si. This type precipitate, which was very rare, is probably a silicate.

3) Splat Cooled 316 SS + 24500 appm Boron

In this alloy, boron exists as a major alloying element (0.5 wt. %). In addition to precipitates similar to those found in specimens with 100 and 500 appm boron content, very small precipitates with a thickness of $\sim$ 200 Å were found only along grain boundaries by using STEM.

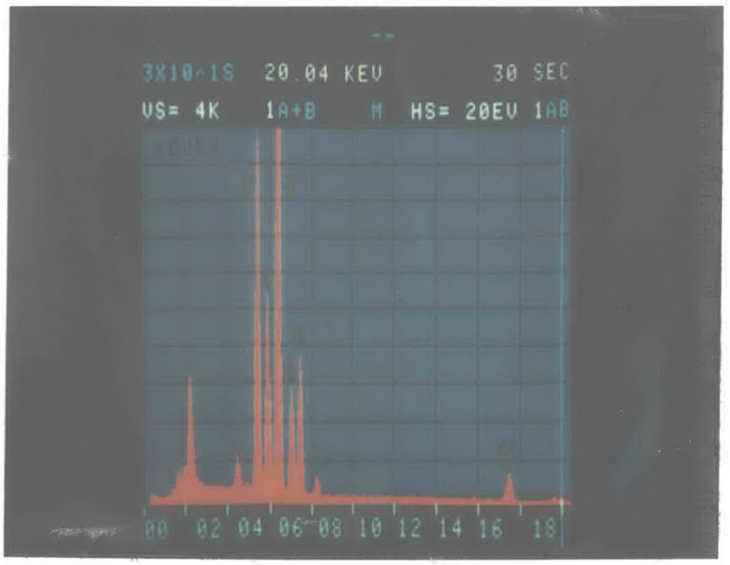

Figure 4.4.--Distribution of elements in a precipitate for 316 SS sample containing 100 appm B: 1) SiK_{α}, 2) MoL_{α}, 3) MoL_{α}, 4) TiK_{α}, 5) CrK_{α}, 6) MnK_{α}, 7) FeK_{α}, 8) FeK_{β}, 9) NiK_{α}, 10) NiK_{β}, and 11) MoK_{α}.

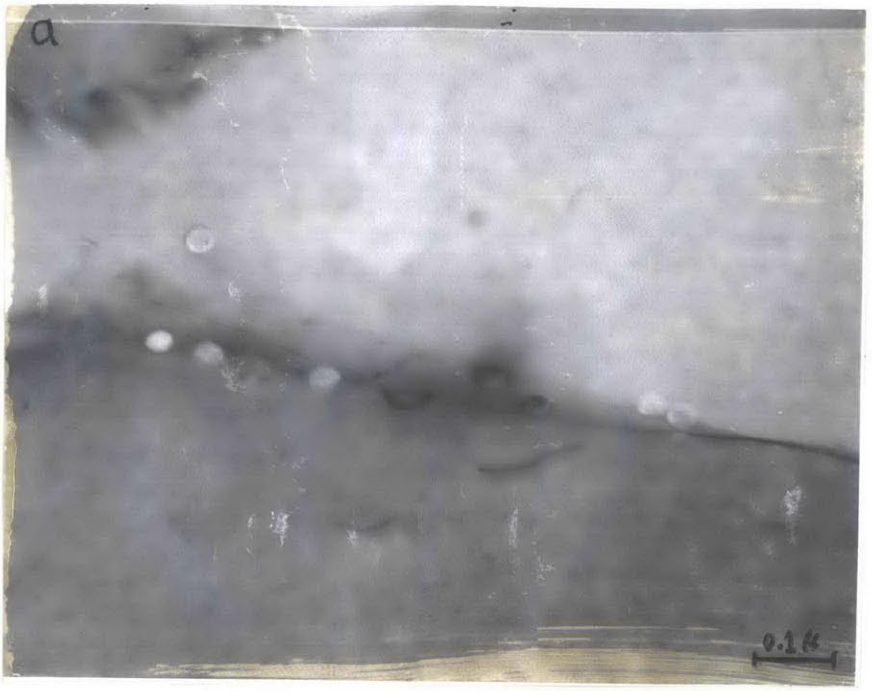

Figure 4.5.--Bright field (a) and dark field (b) STEM micrographs of splat cooled 316 SS containing 500 appm B, 100000x.

These precipitates are completely different from those in specimens with 100 and 500 appm B. Bright field STEM images of a small section of the specimen can be seen in Figure 4.6a. Figure 4.6b shows the result of energy dispersive X-ray analysis of these precipitates. They only contain Mo, Cr, Mn, Fe, and Ni. Chrome and iron are the major elements in the precipitates, corresponding to the two highest peaks. These precipitates are very probable to be boride or boro-carbide. These small precipitates were not found in the splat cooled specimens with 100 and 500 appm B.

All three different specimens have large similar precipitates with Ti and Si in them as well as Cr, Fe, and Ni. The only important difference comes from high boron concentration of 24500 appm (0.5 wt. %) which has resulted in small precipitates rich in Fe and Cr.

4.2 Particle Extraction Method Results

Work has been done on the splat cooled specimens with 100 and 500 appm boron using the STEM and its important attachment, electron energy loss spectrometry. The technique has difficulties in detecting light elements such as boron but it has been able to detect boron in boron nitride[32] (which contains 44% boron). Many precipitates were examined but no boron peak was observed. Microscopic structure of a replica from splat cooled 316 SS with 500 appm B is shown in Figure 4.7. The precipitates are dark in bright field image and

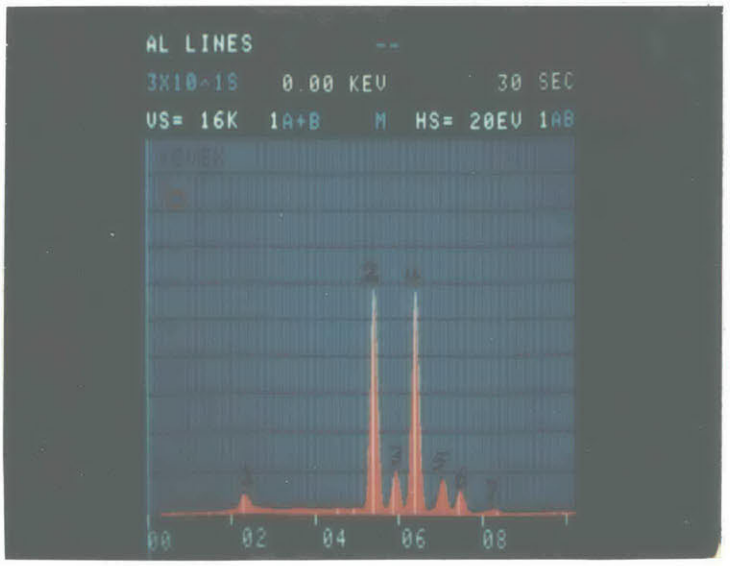

Figure 4.6.--a) STEM microstructure of splat cooled 316 SS + 0.5 wt. % B, 100000x; b) X-ray analysis of precipitates on grain boundaries: 1) MnK_{α} 2) CrK_{α} 3) MnK_{α} 4) FeK_{α} 5) FeK_{β} 6) NiK_{α} 7) NiK_{β}

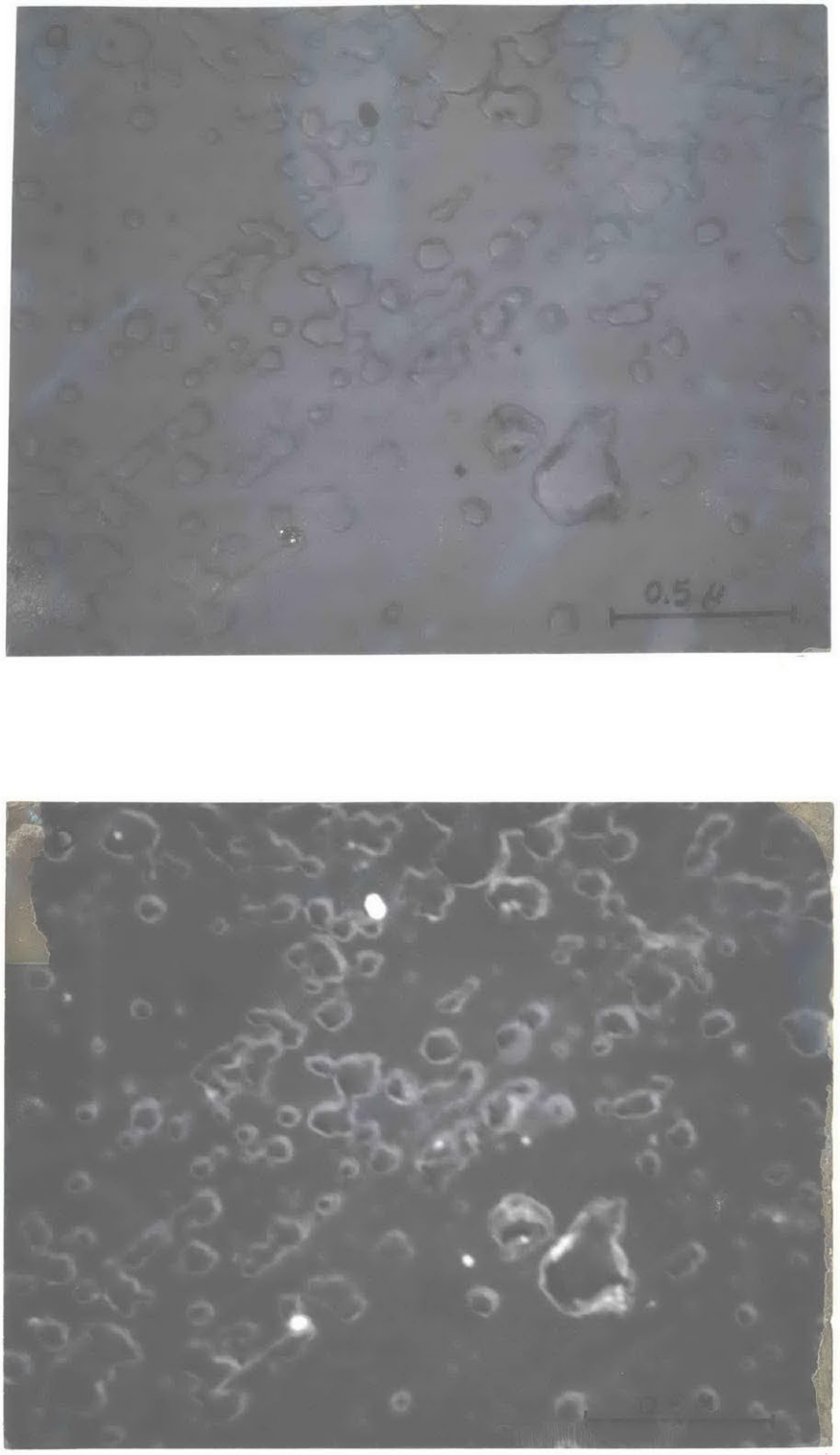

Figure 4.7.--STEM microstructure of an extraction replica of 316 SS with 500 appm B, 50000x; a) bright field, b) dark field.

bright in dark field image.

4.3 Boron Autoradiography Results

Specimens with 100 appm B and 500 appm B and 0.5 wt. % B were studied. Those with 100 and 500 appm B were splat cooled samples with ∿ 2 μm grain size, but specimens with 0.5 wt. % B were conventionally cooled from melt in air, resulting in a grain size of 10-25 μm.

4.3.1 Dependence of Fission Particle Track Size on Etching Time

TEM gives the opportunity to study the effect of etching time on track size. Heat treatment of the plastic film and specimen assembly has also some effect on track size. A two hour heat treatment at 145 ± 2°C was determined to be a good combination of time and temperature. Using this heating condition different etching times were used to study the dependence of track size on etching times. The results are shown in Table 4.2. The etching temperature is 50 ± 2°C.

Table 4.2.--Variation of damage track size with etching time.

Etching time (min)	2	5	7
Track size (μm)	under-etched	under-etched	under-etched
Etching time (min)	10	20	30
Track size (μm)	∿ 0.2 μ	∿ 0.6 μ	∿ 0.8 μ

For high resolution autoradiography, 2 hours heat treatment at

145°C and a 10 minute etch at 50°C are a satisfactory combination.

4.3.2 Track Density

Track density depends on two important parameters, boron concentration and thermal neutron fluence. Track density can be easily found by counting the number of tracks in a selected area. The linear dependence of track density on the product of $\dot{N}_B\phi_{th}t$ was apparent. The relation can be expressed as

$$\rho_t \simeq 8 \times 10^{-15} \dot{N}_B\phi_{th} \cdot t \quad (\text{tracks/cm}^2).$$

$\dot{N}_B$ is the boron concentration (appm). This result is consistent with other results.[18]

4.3.3 Boron Distribution

Boron distribution using plastic replicas was studied by optical microscopy, scanning electron microscopy, and transmission electron microscopy. First, an optical microscope was used to study boron distribution in the splat cooled samples. Because of the limited resolution of the optical microscope ($\sim$ 1-2 μ), it is apparent that we see a uniform boron distribution in such a microscope for splat cooled specimens. Figures 4.8 and 4.9 show the distribution of boron in samples with 100 appm and 500 appm boron, respectively. The resolution of $\sim$ 2 μ is a good one, if the grain size is much larger than 2 μ. In this case, boron distribution

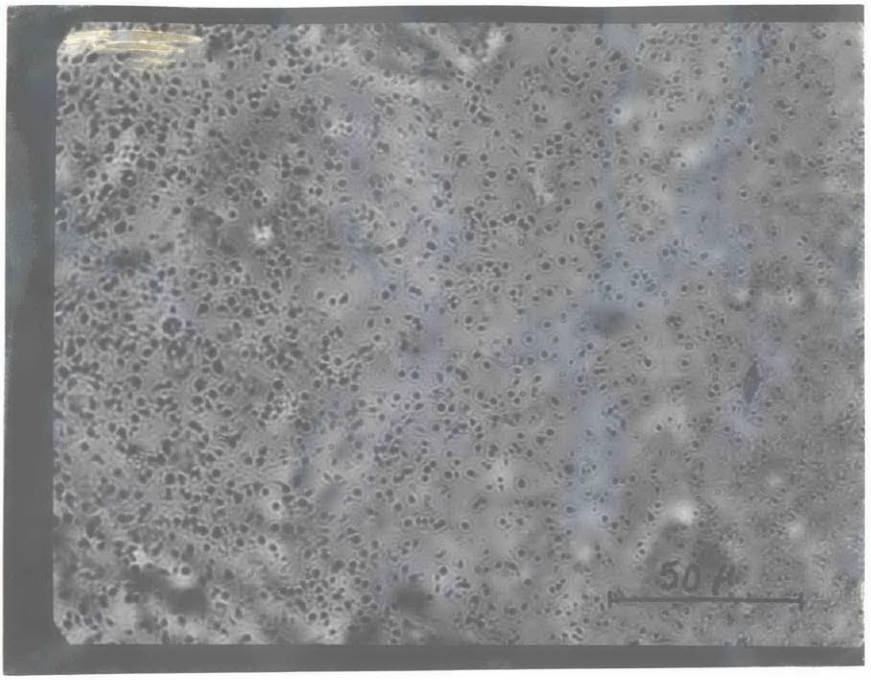

Figure 4.8.--Boron autoradiograph of splat cooled 316 SS with 100 appm B taken by an optical microscope. The fluence is 9.6×10^{13} n • cm^{-2}, 500x.

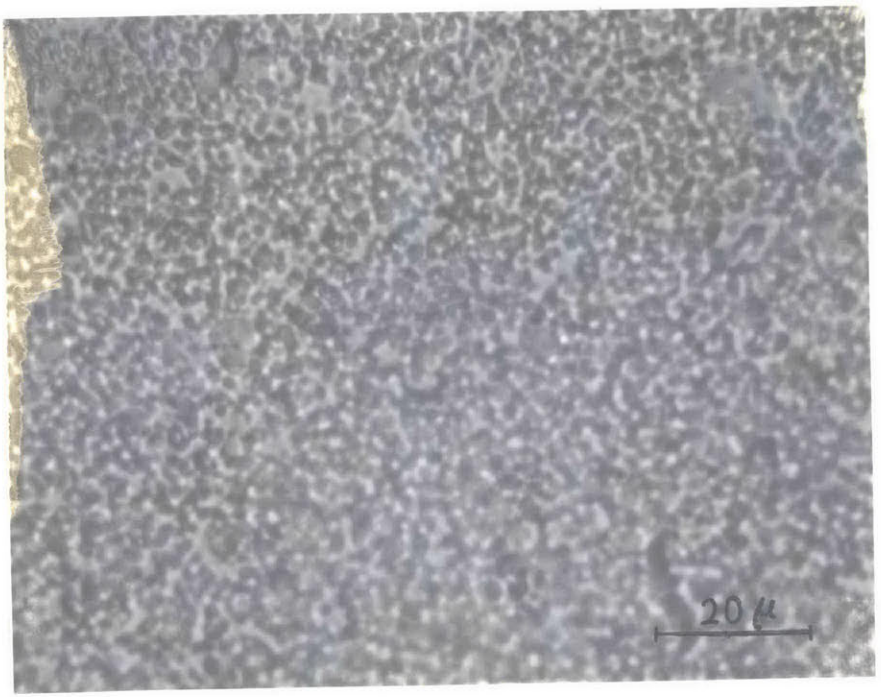

Figure 4.9.--Boron autoradiograph of splat cooled 316 SS with 500 appm B taken by an optical microscope. The fluence is 7.2×10^{13} n • cm^{-2}, 1000x.

can be easily studied. The result on 316 SS containing 0.5 wt. % boron which has been cooled in air is shown in Figure 4.10 at two different magnifications. Boron segregation to grain boundaries is clearly demonstrated.

A much better resolution was obtained when an SEM was used. Figure 4.11 illustrates boron segregation to grain boundaries in an air cooled 316 SS containing 0.5 wt. % boron. The conditions are the same as those used for boron autoradiographs in Figure 4.10. The track size is less than 0.7 μ and the minimum distance between two distinguishable tracks is ∿ 0.5 μ which is considered to be the resolution of the SEM. The plastic replica is unstable in the SEM especially at high voltages. This difficulty limits the resolution because the optimum resolution is obtained at the highest voltage.

A resolution of ∿ 0.3 μ is obtained if a TEM is used. In the TEM, specimens are more stable than in the SEM, but still there is some instability especially at high magnifications. Figure 4.12 illustrates boron autoradiographs of the same sample used for Figure 4.11. Another air cooled 316 SS specimen containing 0.5 wt. % boron was irradiated for only 30 sec and the plastic detector was etched for 10 min in 50% KOH at 50°C. Boron autoradiographs of this specimen observed in the TEM are shown in Figure 4.13. This demonstrates boron distribution very nicely. Thickness of boron rich grain

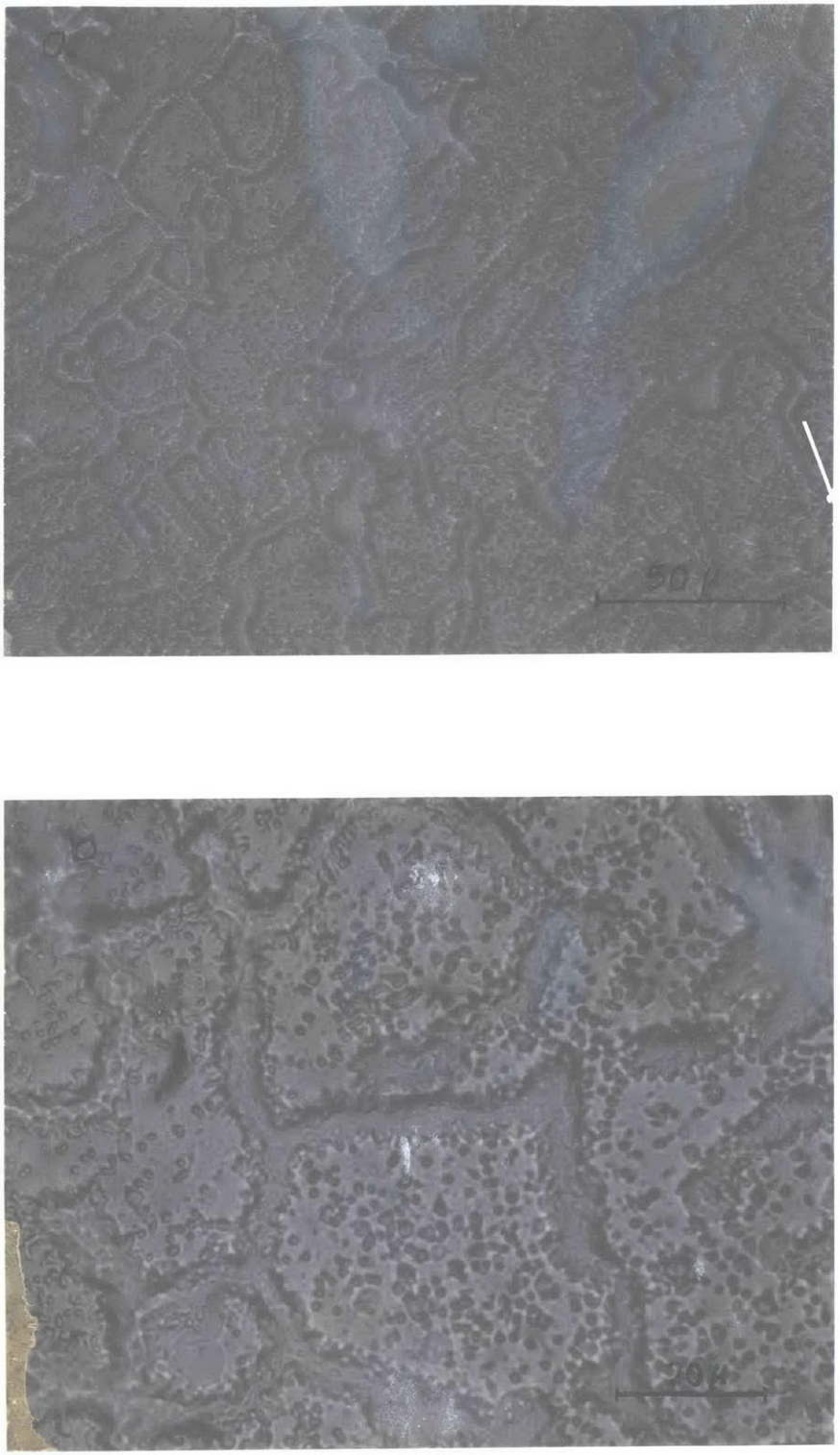

Figure 4.10.--Optical autoradiograph of air cooled 316 SS containing 0.5 wt. % B. The fluence is 6×10^{13} n $\cdot$ cm^{-2}; a) 500x; b) 1000x.

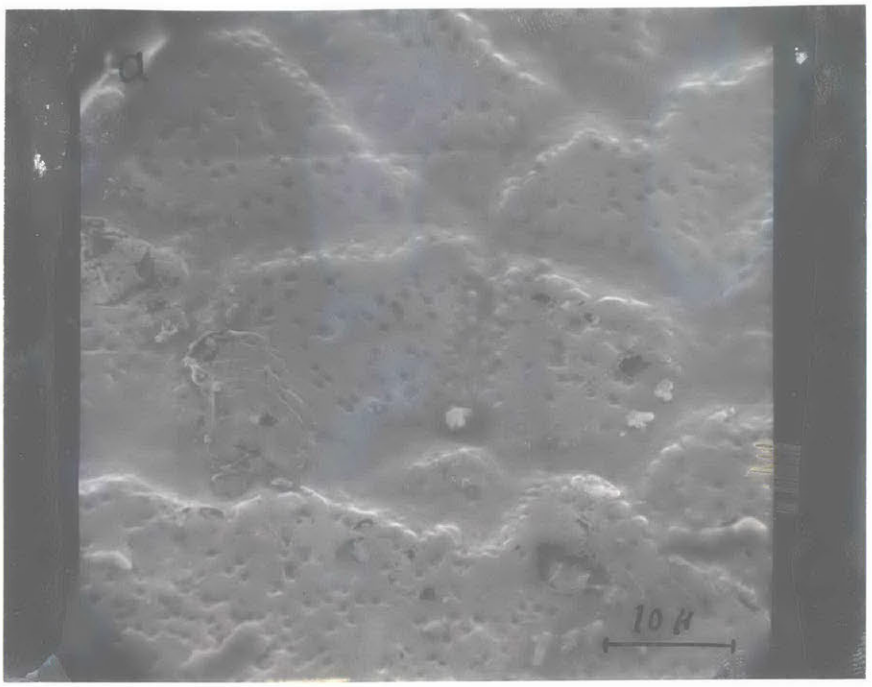

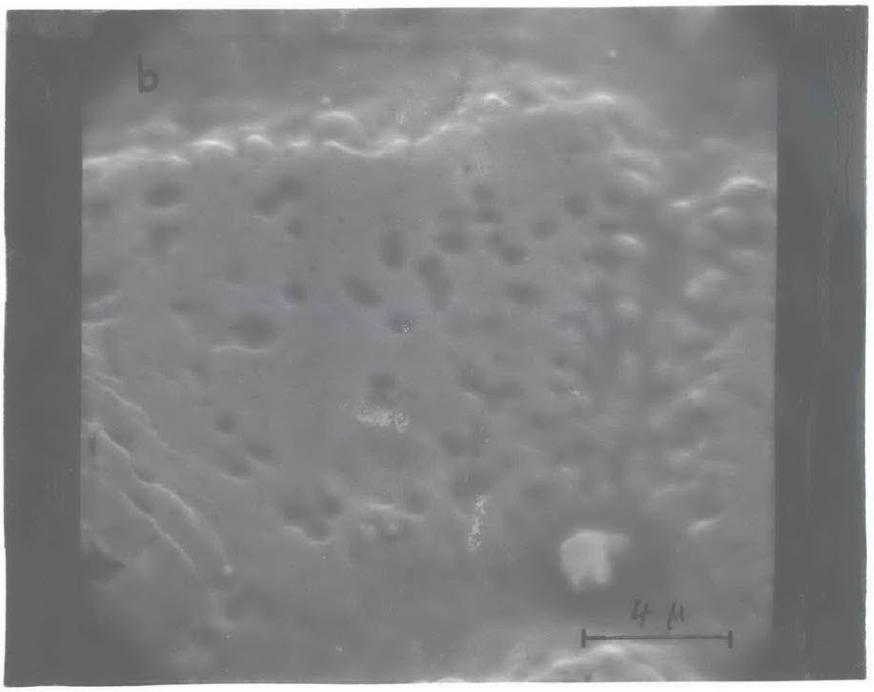

Figure 4.11.--SEM autoradiographs demonstrating boron distribution in 316 SS containing 0.5 wt. % boron. The fluence is 6×10^{13} n $\cdot$ cm^{-2}; a) 1700x; b) 5000x.

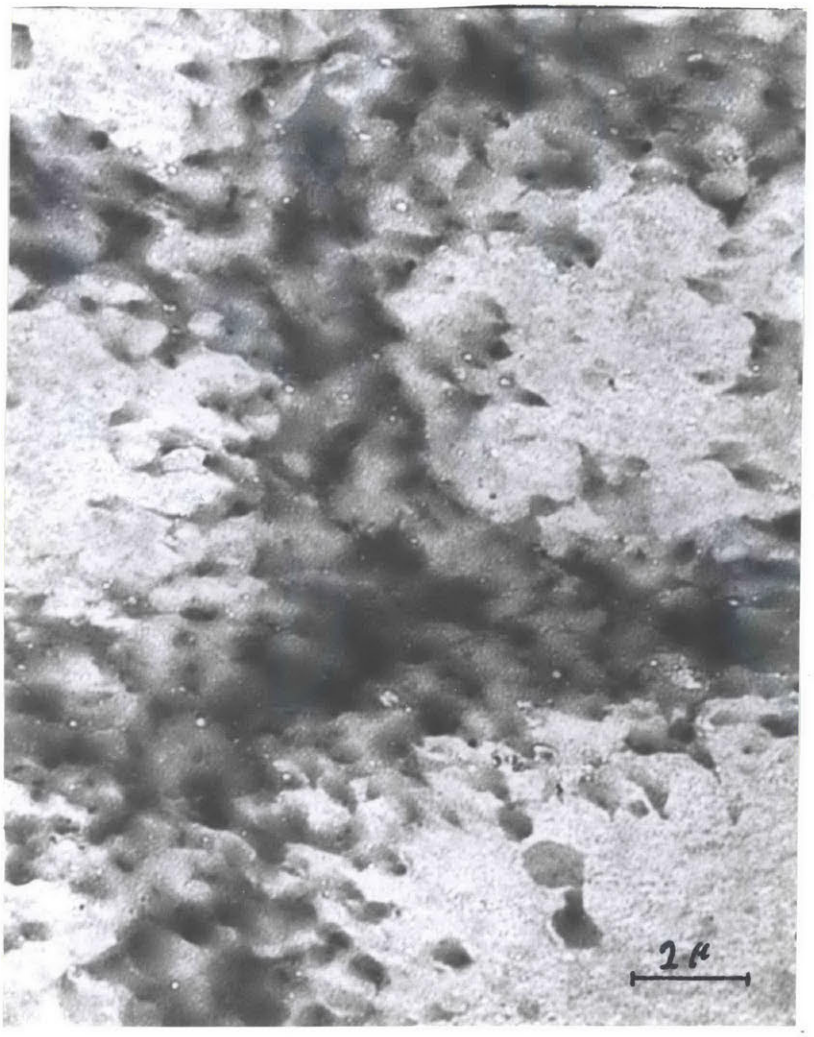

Figure 4.12.--TEM autoradiograph of 316 SS with 0.5 wt. % B. The fluence is 6×10^{13} n $\cdot$ cm^{-2}; 5000x.

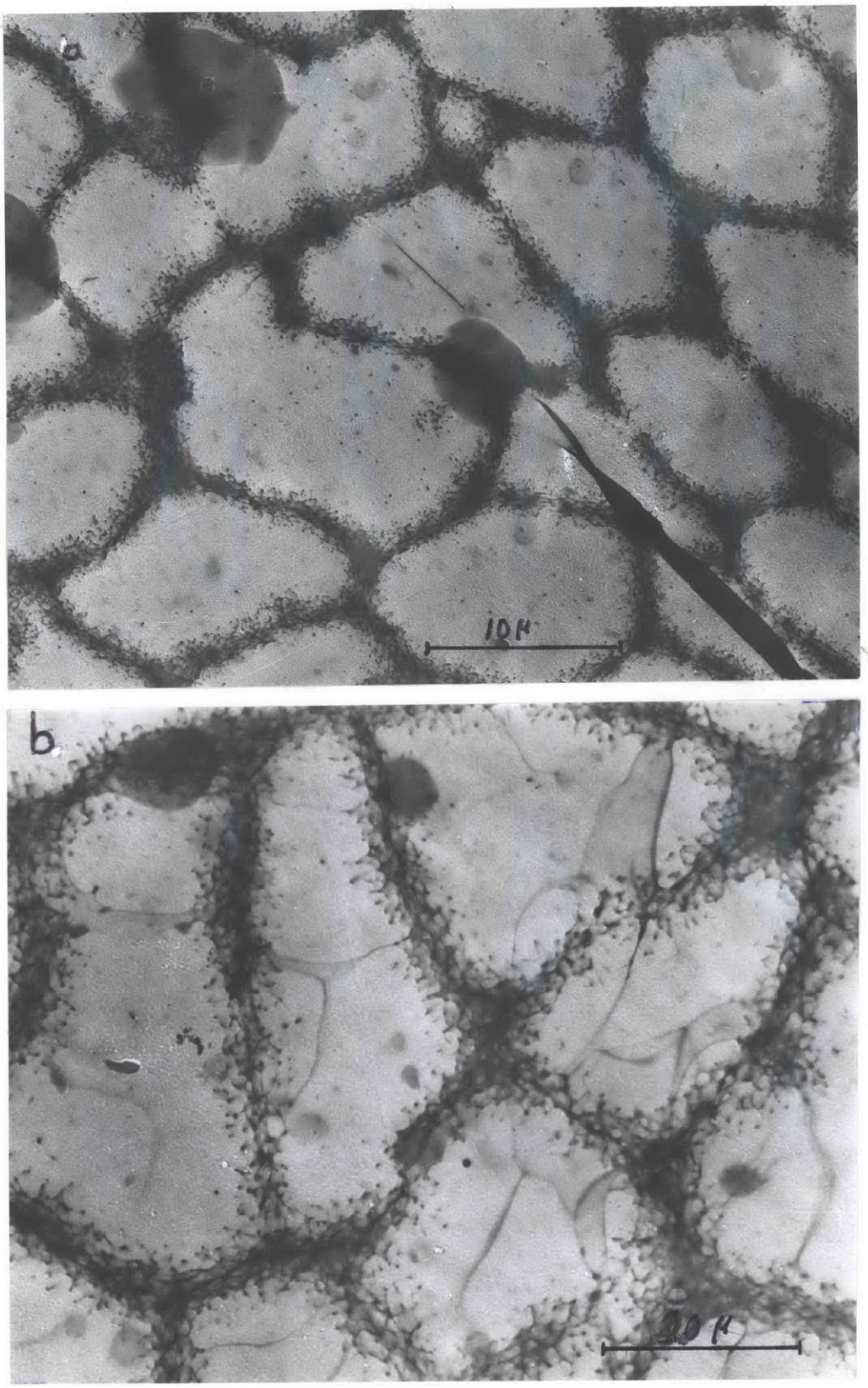

Figure 4.13.--TEM autoradiographs of 316 SS with 0.5 wt. % B. The fluence is 2.4×10^{13} n $\cdot$ cm^{-2}; a) 3000x; b) 6000x.

boundaries is as low as 0.8 μ, proving high resolution of the technique.

With the TEM boron distribution in 316 SS containing 500 appm B was studied. Both air cooled and splat cooled samples were used. Some of the specimens were heated for 90 min at 575°C. No boron segregation was observed in any of the specimens, even in air cooled samples with a grain size of 10-25 μ. Figures 4.14 and 4.15 illustrate the results for heat treated splat cooled and air cooled specimens, respectively.

4.4 Discussion

Boron autoradiography proves to be a strong tool for the study of the boron distribution in materials. CAB film can detect α-particles with energies in the range of 0.5-2 Mev. The inability of CAB to detect low energy α-particles ($E\alpha < 0.5$ Mev) shows that resolution of the technique is much better than the $\sim$ 2 μ; α-particle range in steels. On the other hand, another study[23] has shown that the particles detected by autoradiography originate from the surface of the sample and not from a thin layer at some distance below the surface. This conclusion shows that the resolution is very high and is in fact limited by track size, which can be as low as 0.3 μm. Therefore, a high resolution of $\sim$ 0.3 μm can be obtained when a transmission electron microscope is used. This high resolution makes it feasible to study boron distribution in alloys with small grain size down to $\sim$ 2 μm. As was

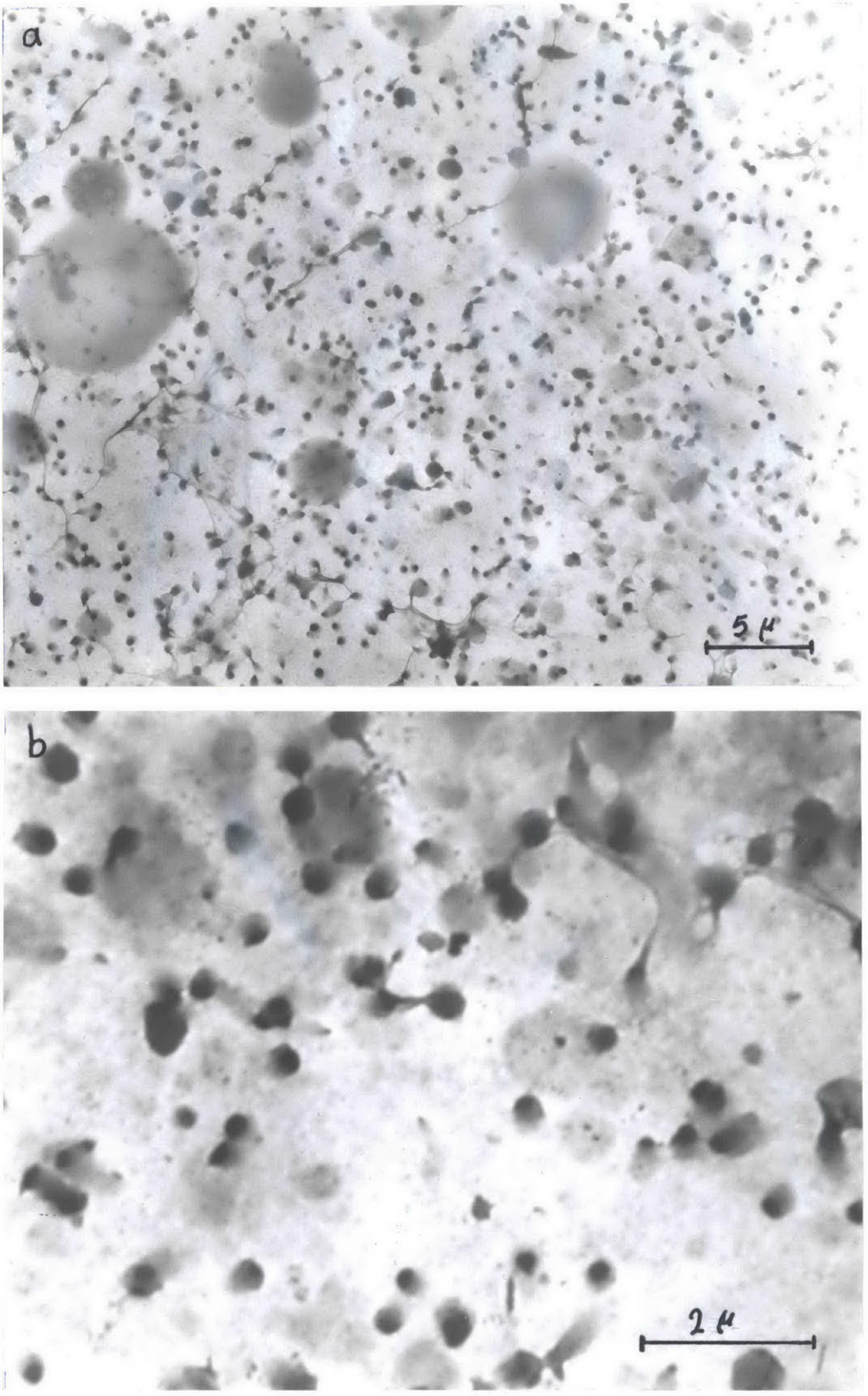

Figure 4.14.--Boron distribution in a heat treated (90 min at 575°C) splat cooled 316 SS; a) 500 appm B, 3000x; b) 100 appm B; 15000x.

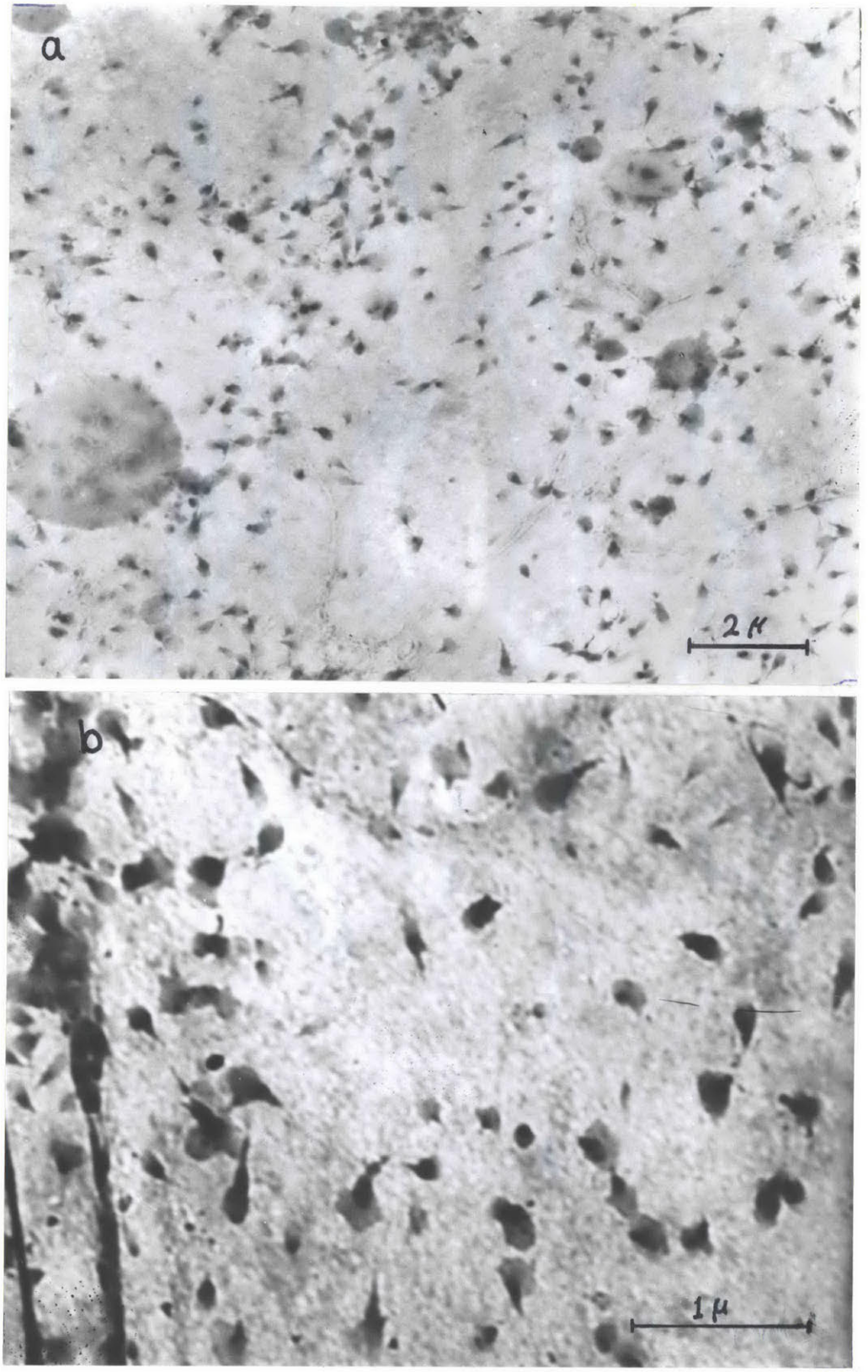

Figure 4.15.--TEM boron autoradiographs of an air cooled, heated (90 min at 575°C) 316 SS with 500 appm B showing uniform boron distribution; a) 9000x; b) 27000x.

mentioned before, the plastic film is unstable in the TEM, but if it is shadowed with a thin layer of carbon or gold, its stability increases. Of course, there is always a possibility to lose the sample in the microscope, therefore great care must be exercised, especially when one is using high magnifications.

Study of stainless steels containing 500 appm B shows that no segregation is obtained even when the sample is cooled in air. This indicates that when 316 SS containing as high as 500 appm B is splat cooled from the melt no detectable boron segregation occurs. The effect of heat treatment has to be studied in details; however, the specimens which were heated for 90 minutes at 575°C showed no sign of segregation, even for air cooled samples with 500 appm B.

Direct examination of 316 SS samples and extraction replicas were made by electron microscopy but were not very successful; nevertheless, the results are in agreement with those for boron autoradiography. The presence of elements such as Si and probably S in the precipitates opposes boron and carbon existence in them. Additional supporting evidence for low boron content in the precipitates comes from the result of electron energy loss spectrometry which didn't detect any boron on the precipitates. These precipitates are probably oxides, sulphides, and silicates formed by the impurities in the specimens.

By using much better material with very low impurity content, one should be able to get rid of these unwanted precipitates. An alloy made from pure Fe, Cr, and Ni might be very useful as an alloy for further study of boron doping in splat cooled materials.

CHAPTER 5

SUMMARY

There are many materials problems associated with the development of fusion power reactors. In order to overcome these difficulties, fusion reactor conditions have to be simulated by running different radiation related tests on the promising materials. Current fission reactors are not capable of such simulation, therefore, researchers have used various tricks to obtain the simulation. A new trick was presented to the U.S. Department of Energy by Professor O. K. Harling, Director of MIT Research Reactor, in which boron doped materials are produced by splat cooling, producing samples with very fine grains of the order of $\sim$ 2 μm in size and hopefully very homogeneous boron distribution. Samples produced in this manner can be irradiated in a mixed neutron spectrum. Radiation damage is produced by the fast neutrons and helium is produced by the thermal neutrons from the $^{10}B(n,\alpha)^{7}Li$ reaction, simulating the fusion reactor environment. This technique is only useful if boron is uniformly distributed in the material; therefore, this research has been carried out to develop a technique for adequately characterizing the boron distribution in fine grained materials.

At present, the most useful technique for boron distribution study appears to be the boron autoradiography technique, in which a sample in contact with a plastic detector is irradiated in a thermal neutron environment. Alpha and lithium particles produced from $^{10}B(n,\alpha)^{7}Li$ reactions enter the plastic film which is placed on the sample. Damage tracks are produced by the fission products. If the plastic film is etched in KOH or NaOH, the tracks will be revealed. Then the film can be studied by microscopy. Distribution of tracks in the plastic film represents the boron distribution in the boron doped alloy. With an optimized combination of etching time and temperature, tracks with a size as small as 0.2 μm are produced. Track distribution can be studied by optical microscopy with a resolution of ∿ 2 μm, but if a TEM is used a resolution of ∿ 0.3 μm can be obtained. This high resolution allows us to study boron distribution in specimens with very small grains.

By this technique, boron distribution in 316 SS with different boron contents was studied. A very severe segregation for air cooled specimens containing 0.5 wt. % B (24500 appm), was observed, but for air cooled specimens with 500 appm B content no segregation was observed. The result was the same for splat cooled specimens containing as high as 500 appm B. Also, no track rich areas were observed for splat cooled specimens. This implies that no boron rich areas exist in splat cooled samples. Figure 5.1 shows a micrograph and an

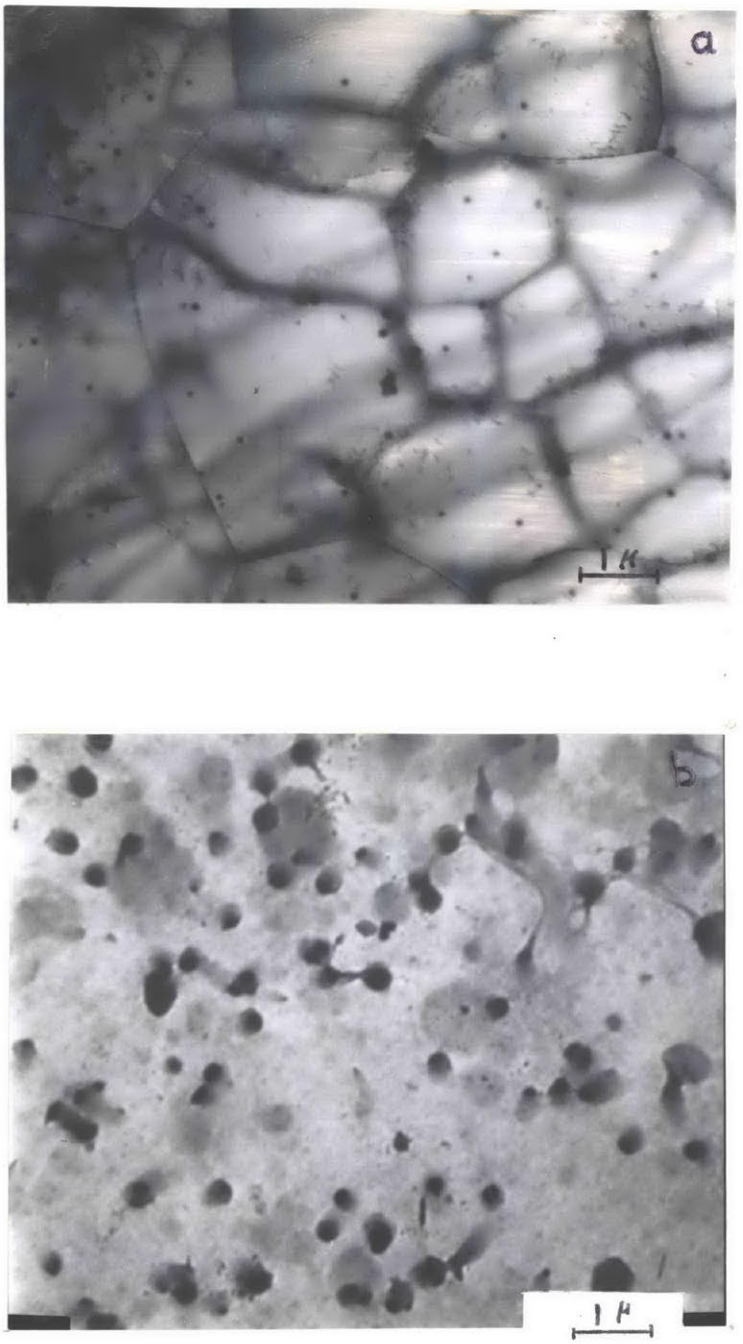

Figure 5.1.--a) A TEM micrograph of a splat cooled 316 SS containing 100 appm B, 10000x; b) Autoradiograph of the same sample, showing boron fission tracks, 10000x.

autoradiograph of a splat cooled 316 SS specimen containing 100 appm B. Table 5.1 summarizes the whole autoradiographic work which has been done on the specimens. As shown in Table 5.1, boron segregation has only been found in air cooled 316 SS containing 24500 appm B. Also optical microscope is not useful for splat cooled materials and an electron microscope must be used for them. The optimum resolution is obtained when the plastic film is etched for 10 minutes in 50% KOH at 50°C. This resolution is $\sim$ 0.3 μm for a TEM.

Electron microscopy was another technique, used to study the microscopic structure of the specimens, and especially to study precipitates. Many precipitates were found in all the specimens. These precipitates were examined by using a combination of STEM and energy dispersive X-ray analysis. Also, extraction replicas were produced and examined by using electron energy loss spectrometry. This was not completely successful, but it supports the autoradiographic result that there is no boron-rich precipitate (boride or borocarbide) in the specimens. The precipitates are probably oxides, sulphides, and silicates, resulting from various impurities in the samples.

There are several other future alternatives for the study of boron distribution in splat cooled steels and other alloys. Electron energy loss spectrometry is under study to make it applicable to the light elements. Secondary ion mass spectrometry and Auger electron spectrometry are two techniques

Table 5.1.--Summary of the boron autoradiographic work done on 316 SS.

Sample	Boron Content (appm)	Preparation	Fluence ($n \cdot cm^{-2}$)	Etching Time in 50% KOH at 50°C	Microscope	Magnification	
Air cooled commercial 316SS	24500	1) The assembly* is heated for 5 hr at 145°C	6×10^{13}	25 min	optical SEM TEM	200-1000x 1000-5000x 2000-20000x	1) Severe boron segregation was observed along grain boundaries. 2) A resolution of ∿ 0.3 μm was obtained in TEM. 3) A track size of 0.2 μm was obtained for etching time of 10 min.
		2) The assembly* is heated for 2 hr at 145°C	2.4×10^{13}	10 min	optical SEM TEM	200-1000x 1000-5000x 2000-20000x	
Splat cooled 316 SS	100	1) The assembly* is heated for 2-5 hr at 145°C	9.6×10^{13} to 4×10^{14}	10-30 min	optical TEM	200-1000x 2000-20000x	1) A uniform track distribution was observed for both cases. Therefore, no boron segregation was observed. 2) Optical microscope was not useful for these samples.
		2) The 316 SS specimen is heated for 90 min at 575°C and the assembly* is heated for 2 hr at 145°C	9.6×10^{13} to 4×10^{14}	5-15 min	TEM	2000-20000x	
Splat cooled 316 SS	500	1) The assembly* is heated for 2-5 hr at 145°C	4.8×10^{13} to 4×10^{14}	10-30 min	optical TEM	200-1000x 2000-20000x	1) Grain boundary segregation of boron was not observed for both cases. 2) Optical microscope was not useful for these samples
		2) The 316 SS specimen is heated for 90 min at 575°C and the assembly* is heated for 2 hr at 145°C	4.8×10^{13} to 4×10^{14}	5-15 min	TEM	2000-20000x	
Air cooled 316 SS	500	1) The assembly* is heated for 2 hr at 145°C	4.8×10^{13} to 4×10^{14}	5-10 min	TEM	2000-20000x	1) In spite of low cooling rate which resulted in large grain size (10-20 μm) no segregation was observed even for the second case.
		2) The 316 SS specimen is heated for 90 min in 575°C, then the assembly* is heated for 2 hr at 145°C	4.8×10^{13} to 2×10^{14}	5-10 min	TEM	2000-20000x	

*Assembly of CAB film and 316 SS specimen.

which should be useful for boron identification. These techniques with high resolution are not now available at MIT, but they will be in the near future. A combination of these techniques with boron autoradiography should provide a very useful tool for studying the boron distribution with a very high resolution, useful for splat cooled materials.

REFERENCES

1. Hirsch, R. L., Proceedings, 1972 International Conference on Nuclear Solutions to World Energy Problems, American Nuclear Society, Hilsdale, Illinois (1973):216.

2. Kulcinski, G. L., Doron, D. G., and Abdov, M. A., ASTM STP 570 (1976).

3. Private communication with Professor O. K. Harling.

4. Elen, J. D., and Glus, A., J. Nucl. Mater. 34 (1970):182.

5. Silk, E. C. H., and Barnes, R. S., Phil. Mag. 4 (1959):695.

6. Abdullaev, K. H., Gorbachev, S. K., Perelygin, V. P., and Treitiakova, S. P., "Determination of the Geological Age of Mica by the Tracks of Uranium Fission Fragments," Dubna Preprint 3 (1966):2961.

7. Stover, B. J., and Jee, W. S. S., "Radiobiology of Plutonium," Salt Lake City, J. W. Press (1972):183.

8. Gregg, R., and Tombrello, T. A., Radiation Effects, Vol. 00 (1977):paper 131.

9. Weller, R. A., and Tombrello, T. A., Radiation Effects, Vol. 00 (1978):paper 022.

10. Ollerhead, R. W., Mann, F. M., Kneff, D. W., Switkowski, Z. E., and Tombrello, T. A., Physical Review Letters 36-8 (1976):439.

11. Fleischer, R. L., Price, P. B., and Walker, R. M., "Nuclear Tracks in Solids," University of California Press (1975).

12. Brownrigg, A., "Boron in Steel," J. Aust. Inst. Met. 18-3 (1973):124.

13. Grovnes, M., J. Mat., SMLSA, 3, 3 (1968):614.

14. Lagerquist, M., and Lagneborg, R., Scand. J. Met. 1 (1972):81.

15. Williams, T. M., Harries, D. R., and Furnival, F., J. Iron and Steel Inst. (May 1972):351.

16. Hellstrand, E., Lagneborg, R., Lindbagen, P., Westin, R., and Ostberg, G., J. Nucl. Mat. 48 (1973):1.

17. Hughes, J. D. H., and Rogers, G. T., J. Inst. Met. 95 (1967):299.

18. Kawasaki, S., Hishihuma, A., and Nagasaki, R., J. Nucl. Mat. 39 (1971):166.

19. Tanaka, M., and Kawasaki, S., J. Nucl. Mat. 48 (1973):366.

20. Elen, J. D., and Glas, A., J. Nucl. Mat. 48 (1973):36.

21. Hughes, J. D. H., Dewey, M. A. P., and Briers, G. W., Nature 223 (1969):498.

22. Garnish, J. D., and Hughes, J. D. H., J. Mat. Sci. 7 (1972):7.

23. Garnish, J. D., and Hughes, J. D. H., J. Inst. Met. 10 (1973):108.

24. Derytter, A. J., and Pelfer, P., J. Nucl. Energy 21 (1967):83.

25. Kaye, G. W. C., and Laby, T. H., "Table of Physical and Chemical Constants," 13th Ed. (Longmans, Harlow, 1966).

26. Price, P. B., and Walker, R. M., J. Appl. Phys. 33 (1962):3407.

27. Desorbo, W., and Humphrey, J. S., Jr. Radiation Effects 3 (1970):281.

28. Heckmen, H. H., Perkins, B. L., Simons, W. G., Smith, F. M., and Barkas, W., Phys. Rev. 117 (1960):544.

29. Linhard, J., Scharff, M., and Schiott, H. E., Kgl. Danske Videnskab. Selskab, Mat. Fys. Medd 33,14 (1963):1.

30. Fain, J., Monnin, M., and Montret, M., Rad Research 57 (1974):379.

31. Von Borries, B., Z. Naturf. 4a (1954):52.

32. Private communication with Dr. E. Hall.